A Regulatory Loop between the Retinoid-Related Orphan Nuclear Receptor NHR-23 and *let-7* family microRNAs Modulates the *C. elegans* Molting Cycle

Ruhi Patel[1] and Alison R. Frand[1]*

[1]Department of Biological Chemistry
David Geffen School of Medicine
University of California, Los Angeles
Los Angeles, CA 90095

*To whom correspondence should be addressed: afrand@mednet.ucla.edu

Keywords: circadian clocks, developmental timers, behavioral quiescence (sleep), oscillatory gene expression, *Period*, *Per2*, *lin-42*

Abbreviations:

UTR	Untranslated Region
RNA	Ribonucleic Acid
RNAi	RNA interference
ROR	Retinoid-related Orphan Receptor
HRE	Hormone Response Element
NHR	Nuclear Hormone Receptor
PER	PERIOD gene
GFP	Green Fluorescent Protein
iCLIP	Individual-nucleotide resolution Crosslinking Immunoprecipitation
RORE	ROR Response Element
LCS	*let-7* consensus site
NHR	Nuclear Hormone Receptor
Mlt	Molting Cycle Defective
MFE	Minimum Free Energy
pri	Primary
Let	Lethal
CRISPR	Clustered Regularly Interspersed Short Palindromic Repeats
crRNA	CRISPR RNA
tracrRNA	Trans-activating crRNA
nt	Nucleotides
td	Tandem
ssODN	Single Stranded Oligodeoxynucleotides
VPC	Vulval Precursor Cell

SUMMARY

Animal physiology and development both rely on biological clocks, but the extent to which feedback loops among core components of the circadian clock and conserved microRNAs operate within developmental timers is not well understood. Here, we show that a negative feedback loop between NHR-23/RORα and *let-7* modulates the PER-dependent rhythm of the *C. elegans* molting cycle. Related quiescent intervals are delayed and protracted in *nhr-23* knockdowns, advanced and abbreviated in particular *let-7* mutants, and yet scheduled more regularly in double mutants. NHR-23 binds upstream ROR Response Elements (REs) and activates transcription of primary *let-7* when larvae are active, whereas *let-7* targets an LCS in the 3′UTR and represses expression of *nhr-23* transcripts when larvae are quiescent. Moreover, NHR-23 and *let-7* have scores of shared targets that are cyclically expressed and mediate related transitions in cell and animal behavior. ROREs are also found upstream of vertebrate *let-7* homologs, while LCSs are found in 3′UTRs of *ROR* transcripts. Conservation of this feedback loop has implications for human clocks and related malignancies and disorders of sleep and metabolism.

INTRODUCTION

Timekeeping and time management are biological imperatives. Distinct timers govern key features of rhythmic events during development such as the time interval between each event and the number of times the event is repeated. Some examples are the developmental timers that regulate the segmentation of insects and the formation (and segmentation) of vertebrate somites (El-Sherif et al., 2012; Gomez et al., 2008). Mutations that affect principal components of the somitogenesis clock can cause neonatal mortality (Matsu-Ura et al., 2016; Sparrow et al., 2007).

The circadian clock, which coordinates sleep-wake cycles and other physiologic rhythms with the solar day, is perhaps the best-characterized biological timer. Moreover, core components of the circadian clock, such as PERIOD, also regulate behavioral and seasonal rhythms — the periods of these rhythms range from milliseconds to months. Mutations that affect core components of the circadian clock cause acute sleep disorders, metabolic syndromes, and malignancies, underscoring the significance of the circadian clock to human health (Oyama et al., 2017; Patke et al., 2017; Puram et al., 2016; Roenneberg and Merrow, 2016).

Interconnected positive and negative transcriptional–translational feedback loops (TTFLs) are the mainstay of clock biology (Takahashi, 2016). The transcriptional activators CLOCK and BMAL1 and their repressor PERIOD are core components of the circadian clock. Retinoid-Related Orphan Receptors (ROR) activate the expression of *BMAL1*, integrating organ-specific and CNS clocks (Cook et al., 2015; Zhang et al., 2017). Recent studies have uncovered microRNA-mediated, post-transcriptional feedback loops that modulate the circadian clocks of peripheral tissues. The breadth and significance of these regulatory loops to the assortment of physiologic and developmental timers remain unclear.

PER proteins also regulate the molting cycles of both arthropods and nematodes (Olmedo et al., 2017). *C. elegans* molt 4 times at regular intervals, once every 8–10 h under typical culture conditions. The process of molting involves separation of the existing cuticle from the epidermis (apolysis) and replacement with a larger cuticle for the upcoming life stage. Episodes of behavioral quiescence (lethargus) accompany renovation of the integument and last 2–3 h. Lethargus is now considered a model for sleep based on shared features such as neuroendocrine regulation, sensory depression and homeostatic drive (Trojanowski and Raizen, 2016).

Finding that LIN-42, the *C. elegans* counterpart of insect and mammalian *Period*, is required for worms to molt at regular intervals implied the existence of a molting cycle timer ancestrally related to the circadian clock (Jeon et al., 1999; Monsalve et al., 2011). Levels of *lin-42* transcripts cycle in time with the molts, as do levels of this transcriptional repressor seen in the nucleus. Additional components of the molting timer – especially regulators of gene expression – were anticipated but not identified.

One candidate was the orphan nuclear hormone receptor NHR-23, the one and only worm homolog of vertebrate RORs (Antebi, 2015). The *nhr-23* gene itself is required for completion of the molts and is transiently but repeatedly expressed in the epidermis during each larval stage. Moreover, NHR-23 directly or indirectly promotes the expression of many downstream targets linked to the molting process. (Frand et al., 2005; Kouns et al., 2011).

The *let-7* family of miRNAs (hereafter *"let-7s"*) were also logical candidates for components of the molting cycle timer. Historically, the *let-7* gene was first characterized during studies of the heterochronic pathway, which specifies successive temporal fates manifest by the epidermal stem (seam) cells of *C. elegans* (Ambros and Ruvkun, 2018; Reinhart et al., 2000). The *let-7* miRNA promotes the larval-to-adult transition, while the paralogs *mir-48* and *mir-241* together specify the L2 fate (Abbott et al., 2005). A third paralog, *mir-84,* appears to act cooperatively with *let-7*, *mir-48,* and *mir-241* across development. The *let-7s* are recognized effectors of the number of molts but not the pace of the molting cycle. However, primary *let-7s* transcripts are cyclically expressed in phase with the molts in the seam cells, which repeatedly alternate between division and quiescence in coordination with the molting cycle (Van Wynsberghe et al., 2011).

Genetic interactions among NHR-23, let-7, and LIN-42 were uncovered in prior studies. Specifically, *let-7* suppresses supernumerary molts by directly or indirectly repressing both *nhr-23* and *nhr-25*, which is a homolog of SF-1 (Hayes et al., 2006). Moreover, a feedback loop between *lin-42/Per* and *let-7 was* uncovered by co-suppression of heterochronic phenotypes and further molecular analyses (McCulloch and Rougvie, 2014; Perales et al., 2014; Van Wynsberghe et al., 2014). The extent, if any, to which the abovementioned interactions affect the biorhythm of molting was not clear.

Here, we show that both *nhr-23* and *let-7s* modulate the biorhythm of molting, exerting opposing but co-dependent effects on the pace of larval development. Explicating this, we show that NHR-23 activates expression from the promoter of *let-7*, whereas *let-7s* dampen the pulsatile expression of *nhr-23* transcripts from the L2 stage through adulthood. Further, we identify scores of shared targets of both NHR-23 and *let*-7s, each of which is cyclically expressed and linked to the process of molting. Evidence that the feedback loop between NHR-23/RORα and *let-7s* is conserved in vertebrates has clear implications for human clocks and related malignancies along with disorders of sleep and metabolism.

RESULTS

Opposite effects of *nhr-23* and *let-7s* modulate the biorhythm of molting.

Newly hatched *C. elegans* larvae undergo four molts at regular 8-10 h intervals prior to emergence in the adult stage (Figure 1A). As such, L1 larvae simultaneously released from starvation-induced diapause and cultivated with food subsequently complete the molts in concert. To quantify and compare the biorhythms of selected strains versus wild-type *C. elegans* (N2), we systematically observed individual worms at regular 1 h intervals, videotaping for 15 s on the hour. The subjects composed isogenic cohorts developing from the 2nd to 3rd larval stage (L2 to L3), from the 3rd to the 4th larval stage (L4), and from the 4th larval stage to adulthood. Active worms were identified by locomotive (sinusoidal) body movements and pharyngeal muscle contractions (pumps). Recorded frequencies of pumps were measured *post hoc* and graded as high, medium, or low on a scale set by the mean and standard deviation of age-matched, wild-type worms. Lethargic worms were identified by the absence of detectable pumps or locomotion, combined with a rectilinear or hockey stick-like body posture (Iwanir et al., 2013; Raizen et al., 2008). Separation of the preexisting cuticle from the body and detection of its remnants on the culture plate signified the commencement and completion of ecdysis (Singh and Sulston, 1978).

The actograms in Figure 1B display records from key longitudinal studies in reverse chronological order. As anticipated, cohorts of wild-type larvae passed through active and lethargic intervals practically in sync. For instance, wild-type animals were active for 8.1 ± 0.5 h (mean ± sd) during L4 and lethargic for 2.2 ± 0.4 h during the L4/adult molt. Afterward, wild-type adults escaped from the outmoded cuticle and

quickly recommenced the abovementioned activities. Supplemental Table 1 specifies both the active and lethargic interval along with the wake-to-wake interval — defined as the time elapsed between two chronological transitions from dormancy to activity — for each experimental cohort.

To evaluate the potential regulatory role of NHR-23, we used bacterial-mediated RNA-interference (RNAi) to knockdown *nhr-23* in larvae (Timmons et al., 2001). Rescheduling the initial delivery of *nhr-23* siRNAs circumvented larval arrest and lethality prior to the stage of interest. For example, to observe *nhr-23* knockdowns during L4, hatchlings were cultivated on mock bacteria for 14 h and then transferred to bacteria that expressed *nhr-23* dsRNAs. In addition, only larvae that completed the L3/L4 molt were included in the longitudinal study (see STAR Methods). Following this regimen, all *nhr-23(RNAi)* larvae appeared superficially normal at the start, but none had fully shed the outmoded larval cuticle at the end of the experiment (the Mlt or Molting defective phenotype).

L4-stage *nhr-23(RNAi)* animals were active ~20 min longer and lethargic 2.4 ± 0.8 h longer than mock-treated wild-type animals. L3-stage *nhr-23(RNAi)* larvae were active 1.4 ± 1.3 h longer and lethargic 2.2 ± 1.9 h longer than control animals (Figure 1B′). In this study, one *nhr-23(RNAi)* larva was quiescent during 9 consecutive time samples. An L2-stage cohort of *nhr-23(RNAi)* larvae was lethargic for 2.6 ± 1.2 h longer than wild-type larvae. This lengthy delay coincided with the most potent knockdown of *nhr-23*, as indicated by qRT-PCR (see STAR Methods). Thus, delayed and protracted sleep-like phases were associated with knockdown of *nhr-23* during three successive life stages.

The majority of *nhr-23(RNAi)* animals also appeared sluggish after awakening from lethargus. In principle, incomplete remodeling of the pharyngeal cuticle could account for diminished pumping rates. Alternatively, knockdown of *nhr-23* could lead to less robust and/or irreversible transitions from quiescence to activity.

To determine whether *let-7s* also regulate the biorhythm of molting, we tracked cohorts of both *let-7(n2853)* and *let-7(mg279)* animals using the same approach. Both mutations are associated with lower levels of mature *let*-7 relative to wild type. However, *n2853* is a substitution in the seed sequence, whereas *mg279* is a 27-bp deletion upstream of the mature miRNA (Bracht et al., 2004; Reinhart et al., 2000). The cohort of *let-7(n2853)* animals progressing from L4 to adulthood entered lethargus 1.8 ± 0.6 h earlier and reawakened 0.7 ± 0.6 h faster than wild-type animals (Figure 1B). A distinct

L4 cohort of *let-7(n2853)* animals isolated from a second strain also developed faster. In both experiments, *let-7(n2853)* animals ruptured 1 to 6 h after ecdysis—a hallmark of strong loss-of-function alleles caused by abnormal morphogenesis of the vulva (Ecsedi et al., 2015). The cohort of *let-7(n2853)* larvae progressing from L3 to L4 became lethargic 0.7 ± 0.7 h earlier and reawakened ~0.3 h faster than wild-type animals (Figure 1B′). All but one *let-7(n2853)* worm went on to complete the subsequent molt — outpacing the entire wild-type cohort. Cohorts of *let-7(mg279)* single and *let-7(mg279) mir-84(tm1304)* double mutants progressing from L4 to adulthood became lethargic 0.6 ± 0.8 h and 1.7 ± 1 h earlier than wild-type animals, respectively (Supplemental Table 1). Thus, advanced sleep-like phases were recorded in three distinct *let-7(-)* strains, all of which developed faster than wild-type larvae.

To further characterize genetic interactions between let-7 and NHR-23 relevant to the pace of the molting cycle, we combined *let-7(n2853)* with stage-restricted *nhr-23(RNAi)* and tracked the resulting animals (Figure 1B and 1B′). Both the L4- and the L3-stage cohorts of *nhr-23(RNAi) let-7(n2853)* double mutants remained active longer than *let-7(n2853)* single mutants and reawakened faster than *nhr-23(RNAi)* single mutants, indicating that changes in the biorhythm associated with each single mutant were partially co-suppressed. The corresponding wake-to-wake intervals of *nhr-23(RNAi)* single knockdowns, *let-7(n2853)* single mutants, *nhr-23(RNAi) let-7(n2853)* double mutants, and wild-type animals progressing from L4 to adulthood were: 13.1 ± 1 h, 7.9 ± 0.6 h, 10.6 ± 0.8 h, and 10.3 ± 0.5 h, respectively. A similar trend was observed across the L3-to-L4 molt. Moreover, a triple knockout of the *let-7* sisters partially suppressed the prolonged lethargus caused by RNAi of *nhr-23* during the L2 stage (Supplemental Table 1). RNAi of *nhr-23* also suppressed the rupture of *let-7(n2853)* animals, possibly because NHR-23 normally binds the promoter and activates expression of *lin-41*, the key target of *let-7* germane to integrity of the vulva (Celniker et al., 2009; Ecsedi et al., 2015). Together, findings from the longitudinal studies suggest that feedback among *nhr-23* and *let-7s* modulates the biorhythm of molting.

Considering the abovementioned phenotypes and prior studies of *lin-42* (Edelman et al., 2016; Monsalve et al., 2011), it seems that LIN-42 may be the shared target at the nexus—all three compose the core oscillator. Consistent with this model, NHR-23 occupies the distinct promoters of *lin-42a* and *lin-42b/c in vivo* (Celniker et al., 2009).

Moreover, knockdown of *nhr-23* during the L4 stage abrogated the corresponding pulse in expression of *lin-42* (Supplemental Figure 1). Findings are consistent with the model that NHR-23 and *let-7s* act in opposing limbs of the molting timer, together with LIN-42/PER.

NHR-23 Binds and Repeatedly Activates the Promoter of *let-7*.

One molecular model consistent with the abovementioned results is that NHR-23 directly activates the transcription of primary *let-7*, whereas *let-7* represses the expression of *nhr-23* transcripts. Both ROR and NHR-23 monomers bind the core response element (RORE) 5′-(A/G)GGTCA-3′ to activate gene expression (Kostrouchova et al., 1998; Ueda et al., 2002). Computational searches identified three ROREs within the minimal promoter of *let-7* (Figure 2A), which is necessary and sufficient for robust expression in the epidermis (Johnson et al., 2003). NHR-23 evidently occupies a ~300bp region aligned with the RORE cluster *in vivo* (Celniker et al., 2009). NHR-23 also occupies ROREs identified in the upstream regulatory regions of all three *let-7* sisters (Supplemental Table 3).

To determine the extent to which NHR-23 activates the *let-7* promoter, we compared the expression of a *let-7p::nls-gfp* transcriptional reporter (Kai et al., 2013) in stage-restricted *nhr-23(RNAi)* and mock-treated animals via quantitative fluorescence microscopy. Beforehand, we measured the intensity of GFP in epidermal nuclei of transgenic animals developing from L3 into adults. GFP was barely detectable early in L3 and L4, but the signal intensified throughout both stages and peaked during the subsequent molts (data not shown). Accordingly, transgenic animals were imaged early in the L3/L4 and L4/A molts (Figure 2B and 2C). At both stages, the signal intensity in hyp7 nuclei was 2.3 ± 1.3-times (mean ± SD) lower in *nhr-23(RNAi)* than mock-treated animals. Levels of GFP in seam nuclei were more variable during the L3/L4 than the L4/A molt, possibly due to continuation of the cell cycle. Even so, the average signal intensity in the seam was lower in *nhr-23* knockdowns than mock-treated animals during both molts.

As a complementary approach, we used TaqMan qRT-PCR to measure and compare the levels of both primary *let-7* transcripts and mature *let-7* in L4-restricted *nhr-23(RNAi)* versus mock-treated, wild-type animals. For this purpose, we collected and processed regular 2-h time samples of synchronized populations developing from

L3 to adulthood. Comparable levels of pri-*let-7* were initially detected in both cohorts (Figure 2D). Levels of pri-*let-7* detected in mock-treated animals peaked at mid-L4 — 4.6 times higher than the preceding trough. In contrast, pri-*let-7* levels either decreased or marginally increased in comparable time samples of *nhr-23(RNAi)* animals. Furthermore, levels of mature *let-7* detected in both mock-treated and *nhr-23(RNAi)* animals initially increased during the L3 stage (Figure 2E). However, levels of *let-7* in mock-treated animals increased by another 160% across the L4 stage and L4/A molt, whereas levels of mature *let-7* stagnated in *nhr-23(RNAi)* animals, even though only 35% of *nhr-23(RNAi)* animals were observed to be molting defective under the experimental conditions. Molting-defective larvae were first observed as levels of *let-7* plateaued, consistent with the attribution of both phenotypes to the knockdown of *nhr-23*. Thus, both pulsatile expression of pri-*let-7* and accretion of mature *let-7* partly depend on the function of *nhr-23.*

The 3′UTR of *nhr-23* contains a repressive element complementary to *let-7.*

We next asked whether *let-7*-family miRNAs target *nhr-23* transcripts in developing larvae. Direct inspection of the 868-bp 3′UTR identified four sites partly complementary to *let-7s* (Mangone et al., 2010). One – hereafter, the *let-7* consensus site (LCS) – perfectly complements the 5′ seed region (Figure 3A and Supplemental Table 2). To test the function of these sites, we constructed a suite of bicistronic reporters for post-transcriptional, *cis*-regulatory elements that were housed in extrachromosomal arrays and expressed in transgenic strains (Figure 3B). Briefly, the coding sequence of tandem (td) tomato was fused with the 3′UTR of interest, while the coding sequence of GFP was fused with the 3′UTR of *unc-54*, which is not targeted by *let-7s.* An SL2 trans-splice site bridged the two fusion genes. The promoter of *dpy-7* drove expression of the operon in the hypodermis. Transgenic animals were imaged during the L4/A molt, when both *dpy-7* and mature *let-7* are highly expressed in the epidermis (Figure 3C). Signals from tdTomato were quantified and normalized to signals from GFP within each worm (Figure 3D and 3E). This approach controlled for potential differences in gene expression associated with particular arrays or mosaic animals, rather than the test 3′UTR combined with *tdtomato*.

The 3′UTRs of *unc-54* and *lin-41* were cloned into bicistronic reporters used as negative and positive controls, respectively (Vella et al., 2004). Levels of tdTomato were

conspicuously higher when combined with the 3′UTR of *unc-54,* rather than the 3′UTR of *lin-41*. The corresponding ratiometric (tdTomato/GFP) values were 2.31 ± 0.32 and 0.68 ± 0.19 (mean ± SD). The observed value of 2.3 approached the predicted value of 2.4 for the negative control. This similarity corroborated two presuppositions: 1) that trans-splicing would be nearly 100% effective, and 2) that tdTomato and GFP would have nearly equivalent half-lives in vivo (Supplemental Figure 2).

Normalized levels of tdTomato were 5.7-times lower when combined with the 3′UTR of *nhr-23*, rather than *unc-54.* Any difference in the efficacy of trans-splicing or nonsense-mediated decay of pre-mRNAs could not account for the apparent repression of tdTomato, as no significant difference was detected in the absolute intensity of GFP expressed from either bicistronic reporter (1076 ± 704 a.u. versus 829 ± 392 a.u., respectively). To identify the specific repressive elements(s), we systematically excised each of the four sites partially complementary to *let-7* from the full-length 3′UTR of *nhr-23*, generating four additional bicistronic reporters. Excision of the LCS led to a two-fold increase in the ratio of tdTomato/GFP signals, relative to the average ratio (0.40 ± 0.10) associated with the unaltered reporter for the 3′UTR of *nhr-23* (Figure 3E). Shortening the 3′UTR could not explain the de-repression of tdTomato, considering that three similar 21-nt deletions led to customary or lower levels of tdTomato, as compared with same-day controls. Thus, the 3′UTR of *nhr-23* contains a functional LCS, consistent with the model that *let-7s* bind and repress the expression of *nhr-23* transcripts during the fourth molt and possibly earlier molts as well.

let-7 dampens the expression of _nhr-23_ and the shared target _mlt-10._

We next sought to characterize the relationship between *let-7s* and the oscillatory expression of *nhr-23* during larval development. For this reason, we used CRISPR/cas9 technology to precisely excise the 21-nt LCS from the endogenous *nhr-23* locus (Paix et al., 2015). The resulting allele – *nhr-23(aaa20)* – was out-crossed to the standard N2 strain 3 times. Thereafter we collected *let-7(n2853)*, wild-type, and *nhr-23(aaa20)* samples of ~1,500 worms at regular 2 h intervals—22-50 h after synchronized hatchlings were released from starvation and cultivated on food. RNA was extracted from each sample and the relative abundance of *nhr-23* transcripts determined by TaqMan qRT-PCR (Figure 4A). Anticipating that these three strains might develop at different rates, we counted pumping versus non-pumping worms before collecting each

sample. Lethargic phases were subsequently identified by troughs in the proportion of pumping animals. Related graphs include 14 time samples encompassing three lethargic and two active phases per strain.

Levels of *nhr-23* transcripts waxed and waned as each cohort progressed from L2 to adulthood (Figure 4A and Supplemental Figure 3A). Peaks were detected ~one-third of the way through L2, L3, and L4 in wild-type samples; however, the amplitude declined from one stage to the next, indicative of dampening. Sharper peaks and wider troughs were detected in *let-7(n2853)* animals. Indeed, the curve was ~5-fold steeper, and the amplitude edged upward in successive developmental stages. Moreover, an extra pulse of *nhr-23* expression was detected in *let-7(n2853)* samples, consistent with the onset of a supernumerary molt. Consequently, *nhr-23* transcripts were ~4.8 times more abundant in *let-7(n2853)* than wild-type young adults. Likewise, the expression curve for *nhr-23* was ~3-fold steeper, and the peaks were 1.7 times higher in *nhr-23*(*aaa20)* mutants, as compared with wild-type animals (Figure 4A′). With the extra pulse, *nhr-23* transcripts were ~3.2 times more abundant in *nhr-23(aaa20)* than wild-type adults. An independent trial produced similar results (Supplemental Figure 3A).

We went on to compare the abundance of *nhr-23* transcripts in successive time samples of *mir-241(∆) mir-48(∆) mir-84(n4037)* triple knockouts, *nhr-23(aaa20)* single mutants, and wild-type larvae developing through two lethargic and one active phase — corresponding to L2 (Supplemental Figure 3B). The curves associated with the triple knockout and *nhr-23(aaa20)* were 3 times steeper and, on average, 2.2 times higher in amplitude than the curve seen in wild-type animals. Thus, *let-7* and its paralogs normally restrain the ascent of *nhr-23* transcript levels from the L2 stage through adulthood. Moreover, the LCS functions as a repressive element in physiologic context. Consistent with this finding, ALG-1 is associated with the 3′UTR of *nhr-23* transcripts, as shown by iCLIP Sequencing studies (Supplemental Table 3).

To determine the effect of *let-7(n2853)* and the related deregulation of *nhr-23* on the cyclical expression of a downstream gene directly involved in the process of molting, we further quantified *mlt-10* transcripts in the same time samples (Figure 4B). The *mlt-10* gene encodes the founding member of an unconventional family of apical matrix proteins present in all 5 stage-specific cuticles (Meli et al., 2010). The expression curve for *mlt-10* was 4 times steeper and the peaks 1.8 times higher, on average, in samples of both *let-7(n2853)* and *nhr-23(aaa20)* mutants, as compared with wild-type animals. In

principle, a supernumerary pulse of *mlt-10* expression might have been detected in *let-7(n2853)* and/or *nhr-23(aaa20)* samples collected more than 50 h after release from L1-diapause. As we describe, *mlt-10* is a shared target of both NHR-23 and *let-7*. As such, *let-7* probably dampens its expression by directly targeting *mlt-10* transcripts and also by targeting *nhr-23* transcripts.

How typical is the combination of transcriptional activation by NHR-23 and post-transcriptional repression by *let-7s* among genes linked to the molting cycle? To address this topic, we systematically classified 70 such genes as targets of NHR-23, *let-7*s, both, or neither using bioinformatic approaches and meta-analyses of large data sets. Genes classified as targets of NHR-23 met two of these three criteria: 1) NHR-23 occupied the upstream regulatory region *in vivo* (Celniker et al., 2009), 2) more ROREs were found in regulatory regions than explicable by chance, and 3) inactivation of *nhr-23* led to lower transcript levels, as detected by comparative microarrays (Kouns et al., 2011). Genes classified as targets of *let-7s* met these two criteria: More LCSs were found in the 3'UTR of corresponding transcripts than explicable by chance, and the Argonaute protein ALG-1 bound the 3′UTR in vivo, as detected by iClip (Broughton et al., 2016). By these rubrics, 57% (40/70) of the genes linked to molting were identified as shared targets of both NHR-23s and *let-7s*. Among these shared targets, 88% were previously found to be expressed in cycles with an ~8 h frequency in developing larvae (Hendriks et al., 2014; Kim et al., 2013). In contrast, only 10% (2/20) of randomly selected genes with no known link to molting were identified as shared targets (Figure 4C, Supplemental Table 3). Evidently, joint regulation by NHR-23 and *let-7s* is a signature of protein-coding genes that are both associated with the molting cycle and expressed in correlated waves.

Is the feedback loop between NHR-23/RORα and *let-7s* conserved between nematodes and vertebrates? Using bioinformatic approaches, we identified multiple ROREs upstream of *let-7* homologs annotated in the genomes of humans, mice, and zebrafish. For example, 4-5 ROREs were identified upstream of mammalian *let-7-a*; at most, 3 of these 6-mers could be explained by chance alone (Supplemental Figure 4A). Moreover, we identified multiple LCSs in the 3′UTRs of *ROR* transcripts annotated in the genomes of zebrafish and mammals. Four sites partially complementary to *let-7* were uncovered in the 3′UTR of human RORα – one of which perfectly matched the *let-7* seed (Supplemental Figure 4B). Furthermore, by inspecting the regulatory sequences of

403 human *PER2*, we identified one RORE upstream of the transcriptional start site and two
404 LCSs in the 3′UTR of *Per2* transcripts. The apparent conservation of these cis-
405 regulatory elements suggests that similar feedback loops among RORα, *let-7s,* and
406 PER2 may modulate the expression of all three genes in human tissues.
407
408 **DISCUSSION**
409 The key findings of this report formulate a refined model for the molting timer
410 (Figure 4D-F). Therein, NHR-23/RORα transcriptionally activates *let-7,* the *let-7* sisters
411 and *lin-42/per*, which represses the expression of pri-*let-7* (McCulloch and Rougvie,
412 2014; Perales et al., 2014; Van Wynsberghe et al., 2014). The *let-7*-family post-
413 transcriptionally represses both *nhr-23* and *lin-42*. This set of regulatory interactions
414 compose interconnected positive and negative feedback loops with time delays — the
415 essential framework of biological clocks. In the proposed model, intrinsic differences
416 between the rates of protein versus miRNA biogenesis influence the time intervals
417 needed for levels of NHR-23, LIN-42, and *let-7s* to rise from troughs to effective
418 concentrations.
419 The proposed mechanism accounts for the relative phases and shapes of the
420 expression curves of *nhr*-23 and *let*-7 observed in wild-type animals. As described, peak
421 levels of *nhr-23* decrease through successive larval stages (Figure 4A). Nevertheless,
422 levels of NHR-23 reach 50% of the stage-specific peak early in each stage. However,
423 levels of primary *let-7* reach the same threshold halfway through each larval stage
424 (Figure 4E). This difference – 1.6 h under our experimental conditions – is consistent
425 with activation of the *let-7* promoter by NHR-23 (Figure 4F). In addition, levels of both
426 *nhr-23* transcripts and proteins peak one-third of the way through each larval stage;
427 thereafter, levels of *nhr-23* transcripts descend more rapidly than levels of NHR-23
428 fusion proteins, consistent with miRNA-mediated degradation and/or translational
429 inhibition. Levels of *lin-42* transcripts peak around the same time, if not later than levels
430 of pri-*let-7* (Supplemental Figure 1B).
431 Inflections in the expression curves of NHR-23 and *let-7* further relate to
432 recurrent events in the molting cycle. In the positive limb of the timer, NHR-23 levels
433 ascend as animals commit to a forthcoming molt. In the negative limb of the timer, *let-7s*
434 repress the expression of *nhr-23* and NHR-23 levels fall as animals transit the molt. This
435 repression decelerates the accrual of NHR-23 in the next life stage and delays the onset

of any subsequent molt. Consistent with this model, *let-7(n2853)* mutants were associated with both the steeper ascent of *nhr-23* transcripts and earlier onset of the lethargic phase at the end of L4.

In theory, even small differences in the threshold concentrations of core components needed to regulate specific downstream targets could enable a single timer to illicit orderly waves in the expression of distinct sets of proteins that mediate sequential transitions or events in the molting cycle. For example, the molting timer could control both the onset and termination of lethargus by regulating both sleep-promoting peptides such as *osm-11* and *flp-13* and wake-promoting peptides such as *flp-2* and *pdf-1* (Chen et al., 2016; Nelson et al., 2014; Singh et al., 2011). Other timer-controlled genes encode proteins involved in tissue renovation, such as *mlt-10* (Meli et al., 2010).

The concept that levels of both NHR-23 and *let-7s* must reach target-specific thresholds to effectively promote or repress gene expression is supported by particular findings in this report and also by current knowledge in the fields of gene regulation and chronobiology (Antebi, 2015; Takahashi, 2017). Indeed, the capacity of NHR-23 to activate any specific target might depend on its concentration relative to the number of functional ROREs in the target promoter; the abundance of co-activators, co-repressors, and competitive NHRs; and the availability of as-yet unidentified ligand(s) derived from dietary steroids or exogenous cholesterol (Galles et al., 2018; Santori et al., 2015). The capacity of *let-7s* to silence any specific target might depend on the number of LCSs within the 3′UTR; the abundance of cooperative miRNAs, and the availability of processing factors or RISC components such as Dicer and ALG-1, respectively. Many of these factors change in predictable ways over time, adding layers of complexity to the timing machinery.

The duration of each larval stage and the total number of molts may be integrated at the level of expression of *nhr-23*. In wild type animals, which undergo 4 molts, peak levels of *nhr-23* transcripts dampen from the L1 to the L4 stage; the transcripts are no longer detected in adults. In contrast, in *let-7* mutants, which undergo supernumerary molts, the levels of *nhr-23* transcripts do not dampen throughout development and a supernumerary pulse of *nhr-23* expression is detected in adults. Expression of *nhr-23* in *let-7* mutant adults is necessary for the oncoming

supernumerary molt (Hayes et al., 2006). Thus, dampening of *nhr-23* levels depends on *let-7s* and may count down the total number of molts.

Our findings are consistent with the emerging concept that miRNA-mediated feedback loops increase the robustness of numerous gene regulatory networks and related outcomes, including cell fate decisions, stress responses, and developmental trajectories. In one prominent example, ligand-bound molecules of the *C. elegans* nuclear hormone receptor DAF-12 directly enhance and expedite the expression of *let-7*-family miRNAs, whereas *let-7s* directly repress the expression of DAF-12. These events promote continuous development in favorable environments rather than L3-stage diapause (Bethke et al., 2009; Hammell et al., 2009). Another feedback loop wherein the FOXO transcription factor DAF-16 targets mir-34 and vice versa reinforces the commitment to diapause in response to stressors, including sleep deprivation (Driver et al., 2013; Isik et al., 2016).

This study recognizes and further integrates miRNA-mediated feedback loops within developmental timers. In this context, feedback loops among NHR-23/ RORα, LIN-42/PER, and *let-7* family microRNAs appear to preserve the capacity of cells and developing animals to switch between bi-stable states at regular intervals. This provides a different and authentic perspective of related gene regulatory networks that complements and extends current models and applies to human health and disease.

ACKNOWLEDGEMENTS

The American Cancer Society (RSG-12-149-01-DDC to ARF), the National Science Foundation (IOS# 1258218 to ARF), and the School of Medicine at UCLA supported this research. Some strains were provided by the *Caenorhabditis* Genetics Center (CGC), which is funded by the NIH Office of Research Infrastructure Programs (P40 OD010440). We thank Amy Pasquinelli (UCSD) and John Kim (Johns Hopkins University) for sharing reagents. We also thank John Kim and Ann Rougvie (University of Minnesota) for helpful discussions and critiques of this manuscript.

FIGURE LEGENDS

Figure 1. Longitudinal studies uncover partly interdependent deceleration and acceleration of the molting cycle in *nhr-23(RNAi)* and *let-7(n2853)* animals.
A) Illustration depicts the phases of the molting cycle reiterated during larval development. **B)** Actograms depict the behavioral states of single animals at regular time samples. Time zero corresponds to the emergence of each larva from the prior molt. Each chart combines records from two independent studies. Criteria used to score animals as active (blue) or lethargic (yellow) during regular time samples are described in the text. **B′)** As above for time samples encompassing L3 and part or all of the L4 stage. The strains analyzed were N2, QK059 and MT7626 (not depicted). When cultivated with food for 42 h, 79% of MT7626 larvae and 71% of QK059 larvae developed into young adults, as compared with 12% of N2 worms.

Figure 2. The promoter of *let-7* is trans-activated by NHR-23 during late larval stages. A) Schematic of the *let-7* locus shows the correspondence between the minimal promoter (MP), the cluster of ROREs, and the region occupied by NHR-23 in mid-stage larvae. Gray shading demarcates upstream regulatory sequences; black, transcribed sequences; and red, mature *let-7.* The major transcriptional start site (TSS) for pri-*let-7* is labelled. Coordinates refer to *Ce.* Chr. X, as archived in WormBase v.253. **B-C)** Representative fluorescence and DIC images of the lateral epidermis show nuclear-localized GFP driven from the promoter of *let-7*. Arrows point to hyp7 nuclei; arrowheads, seam nuclei. Asterisks mark dividing seam cells. Scale bars = 20 μm. Adjacent scatter plots show aggregated values from two independent trials. Bars signify

the mean and sd. ****p≤0.0001, **p≤0.01, Ordinary One-Way ANOVA with Bonferroni's correction for multiple comparisons. **D)** Levels of pri-*let-7* determined by TaqMan qRT-PCR. Each value was normalized to *ama-1* transcript levels in the same sample. All values were then normalized to the mean of all 9 mock-treated time samples. Symbols represent the mean and range from two biological replicates. The x-axis indicates time elapsed (h) on food. The underlying bar depicts developmental stages; gray boxes therein signify observed intervals of behavioral quiescence. The times of initial exposure to *nhr-23* siRNAs and the appearance of molting-defective *nhr-23(RNAi)* larvae are indicated. **E)** As above for levels of mature *let-7*, except that each value was first normalized to U18 levels in the same time sample.

Figure 3. Detection of a functional LCS in the 3′UTR of *nhr-23*. A) Predicted pairing between the transcribed LCS and mature *let-7.* Schematic shows the LCS and similar sites in the *nhr-23* 3′UTR, numbered by nt. from the stop codon (black). **B)** Design of bicistronic reporters for 3′UTR-mediated gene regulation. **C)** Representative fluorescence images show tdTomato and GFP co-expressed from bicistronic reporters with the indicated test 3′UTR. The images in each row show the lateral epidermis of one transgenic worm. Arrowheads point to hyp7 nuclei. Scale bar = 10 μm. **D)** Quantitation of related tdTomato/GFP signals observed in two independent experiments. Circles represent the average values from 3 ROIs per worm. Bars signify the mean and sd. N indicates the cumulative sample size. ****p≤0.0001, ***p≤0.001, Ordinary One-Way ANOVA with Tukey's correction for multiple comparisons. **E)** As above, except that ratiometric values were normalized to same-day controls. The full-length *nhr-23* construct is depicted in blue, the deletion constructs in brown.

Figure 4. *let-7* down-regulates *nhr-23* while both NHR-23 and *let-7* regulate many cyclically-expressed genes. A) Oscillating *nhr-23* transcript levels detected by TaqMan qRT-PCR in 2 h time samples of *let-7(n28530)* and wild-type animals passing progressing from L2 to adulthood. Boxes beneath the x-axis – shaded as per the legend – signify lethargic intervals. Values were first normalized to *ama-1* transcripts, which encode RNA polymerase II, within each sample. Values were then normalized to the average of all 14 wild-type time samples. **A′)** As above, with time samples of *nhr-23(aaa20)* animals. Cultures were synchronized by passage through L1 diapause.

Samples of *let-7(n2853)* and *nhr-23(aaa20)* were collected 22-48 h on food; wild-type, 24-50 h on food. Error bars (wild-type values) indicate the range from two qPCR reactions run alongside *let-7(n2853)* and *nhr-23(aaa20)* samples. Supplemental Figure 3 shows data from an independent trial. **B)** Quantitation of *mlt-10* transcript levels in the same samples, by the same methods. **C)** Classification of 70 molting-related genes as targets of NHR-23, *let-7s*, both or neither – based on meta-analyses of published data, bioinformatic searches, and systematic rubrics further described in Supplemental Table 3. **D-F)** Schematics depict three distinct but related findings that together formulate a cohesive model of the molting timer (see Discussion) **D)** Genetic interactions among *nhr-23*, *let-7s*, and *lin-42* constitute interconnected positive and negative feedback loops – the essential wiring of biological clocks. **E)** Overlapping waves of expression of *nhr-23* and *let-7*. Theoretical curves based on data already described and quantitative imaging of an NHR-23::GFP fusion protein (OP43). RNA and proteins levels are expressed as percentages of peak values; time, as fractions of developmental stages. **F)** Proposed correspondence between levels of NHR-23 and *let-7s*, the expression of critical CCGs, and recurrent transitions between active and quiescent states during larval development.

STAR METHODS

Detailed methods are provided in the online version of this paper and include the following:

- KEY RESOURCES TABLE
- CONTACT FOR REAGENT AND RESOURCE SHARING
- EXPERIMENTAL MODEL AND SUBJECT DETAILS
- METHOD DETAILS
    - Working with *C. elegans*
    - RNA-interference (RNAi)
    - Longitudinal Studies of the Molting Cycle
    - Construction of Fusion Genes and Transgenic Strains
    - Editing the *C. elegans* Genome
    - Quantitative Fluorescence Microscopy
    - Isolation of RNA
    - Quantitative RT-PCR
    - Bioinformatic Analyses
- QUANTIFICATION AND STATISTICAL ANALYSIS

SUPPLEMENTAL INFORMATION

The supplemental information for this article includes four figures and two tables.

SUPPLEMENTAL INFORMATION

KEY RESOURCES TABLE

CONTACT FOR REAGENT AND RESOURCE SHARING

Further information and requests for resources and reagents should be directed to and will be fulfilled by the Lead Contact, Alison R. Frand (afrand@mednet.ucla.edu).

EXPERIMENTAL MODEL AND SUBJECT DETAILS

Unique strains of the model nematode *Caenorhabditis elegans* generated by and used in this research are described in the Key Resources Table.

METHOD DETAILS

Working with *C. elegans*

C. elegans were cultivated, observed, transformed and preserved using standard methods (Stiernagle, 2006). Newly-hatched worms were developmentally synchronized by passage through starvation-induced, L1-stage diapause. Hatchlings were isolated by lysis of gravid hermaphrodites in sodium hypochlorite, suspension of eggs in M9 buffer supplemented with 5 µg/mL cholesterol, and incubation for 16 to 24 h with rotational aeration. Hatchlings were released from diapause by plating on solid nematode growth medium (NGM) seeded with *E. coli* OP50-1. One to two hundred larvae were routinely plated on 6 cm NGM plates. Alternatively, ten to fifteen thousand larvae were plated on 10 cm NGM plates seeded with 10X concentrated *E. coli* HT115(DE3), as described below. *C. elegans* were cultivated at 25°C unless otherwise specified.

RNA-interference (RNAi)

Two clones of *E. coli* HT115(DE3) were used for bacterial-mediated RNAi: one transformed with pPD129.36 (a gift from Andy Fire); the other, with a derivative of pPD129.36 containing *nhr-23* coding sequences. The latter clone was obtained directly from the Ahringer library but matches I-3F11 (Source BioScience). Both clones were cultured and fed to *C. elegans* as described (Kamath et al., 2003), except that NGM was supplemented with 8 mM isopropyl β-D-1-thiogalactopyranoside (Laguna Scientific).

To delay silencing of *nhr-23*, L1 larvae were mock-treated for empirically-

625 determined intervals, harvested, washed thrice in M9 and then divided into test and
626 control groups. Test subjects were plated on bacterial lawns that expressed *nhr-23*
627 dsRNAs, while control subjects were re-plated on bacterial lawns that expressed short,
628 dsRNAs unlike any annotated gene in *C. elegans.* Assays involving single worms called
629 for shorter intervals of initial mock-treatment than assays involving thousands of worms
630 per sample. The specific intervals of mock-treatment used in longitudinal studies of
631 worms developing from late L1 to early L3, late L2 to early L4, and late L3 to adulthood
632 were 0, 6, and 14 h, respectively. The intervals of mock-treatment used in studies of
633 gene expression across the same stages were 0, 16, and 24 h. Under the latter
634 conditions peak levels of *nhr-23* transcripts determined by TaqMan qRT-PCR were
635 6.5- and 4.1-times lower in *nhr-23(RNAi)* than wild-type animals harvested during L3
636 and L4, respectively.
637
638 **Longitudinal Studies of the Molting Cycle**
639 Lethargic larvae were isolated from synchronized populations, transferred to
640 individual wells of 12-well NGM plates seeded with *E. coli* HT115(DE3), and observed
641 for 15 s on the hour using a Zeiss M^{2}BioDiscovery microscope. L3 and younger worms
642 were both observed and videotaped at 600-fold magnification; L4 and older worms, at
643 300-fold magnification. As described, each worm was classified as active or lethargic
644 during each time sample based on defined target behaviors. Molting-defective and
645 ruptured animals were also identified using standard criteria. Worms were videotaped
646 using a Sony HDR-XR500V or Nikon D500 camera attached to the microscope. To
647 measure the pumping rate (Hz) of each specimen, the corresponding film was played
648 back 4-times slower in iMovie version 10.11.2. The number of recorded pharyngeal
649 contractions (pumps) was divided by the duration of the film. Three independent
650 assessments of selected films produced values within 95% of the mean, validating this
651 approach. In Figure 1B, wild-type adults pumped at 3.9 ± 1.1 Hz (mean ± sd). Dark,
652 medium, and light blue signify pumping rates ≥2.8 Hz, 1.7–2.8 Hz, and <1.7 Hz,
653 respectively. In Figure 1B', wild-type animals in the L4 stage pumped at 4.0 ± 1.3 Hz
654 (mean ± sd). Dark, medium, and light blue signify pumping rates ≥2.7 Hz, 1.4–2.7 Hz,
655 and <1.4 Hz, respectively.

Construction of Fusion Genes and Transgenic Strains

The sequences of oligonucleotides used in this study are provided in the Key Resources Table. The bicistronic reporters used to detect regulatory elements within 3′UTRs were constructed by Gibson Assembly (NEB) and standard methods. Phusion High-Fidelity DNA Polymerase (NEB) was used to amplify DNA molecules. The resulting plasmids contained the pBR322 backbone of Fire Lab vectors; the *dpy-7* promoter, which corresponds to nucleotides 7,537,914-7,538,219 of *C. elegans* Chr. X (NC_003284); the synthetic intron embedded in primer HM01; the coding sequence for *tandem (td) tomato*, which was isolated from Addgene plasmid #30530 (a gift from Gerhart Ryffel); one of the test 3′UTRs described below; and an *SL2::gfp::unc-54* 3′UTR cassette (a gift from John Kim. The gene-specific 3′UTRs comprised nucleotides amplified from Chr. I (NC_003279) as follows: *nhr-23*, 7,220,953-7,221,820; *unc-54*, 14,855,909-14,856,180; and *lin-41*, 9,334,850-9,335,964. Deletions within the *nhr-23* 3′UTR reporter (cloned in pHR017) were created using a Q5 Site-Directed Mutagenesis Kit (NEB) and verified by Sanger Sequencing (Genewiz Inc.). To generate distinct extrachromosomal arrays harboring each bicistronic reporter, mixtures of the corresponding plasmid (1ng/µl), the co-transformation marker *ttx-3::gfp* (40ng/µl), and filler DNA pRS316 (59ng/µl) were microinjected into the gonads of wild-type hermaphrodites. Transgenic progeny and unique descendent strains were isolated by standard methods.

Editing the *C. elegans* Genome

The CRISPR/Cas9 system was used essentially as described (Paix et al., 2015) to delete the endogenous LCS from the 3′UTR of *nhr-23*, generating the allele *nhr-23(aaa20)*. Briefly, wild-type hermaphrodites were microinjected with a mixture containing the following: *nhr-23* crRNA (400ng/µL), tracrRNA (1µg/µL), *dpy-10* crRNA (160ng/µL, GE Dharmacon), *dpy-10* ssODN (13.75ng/µL, IDT), and CAS9 protein (500ng/µL, PNA Bio) in HEPES buffer pH 7.5 (Sigma-Aldrich) supplemented with 0.025µM KCL (Sigma-Aldrich). Injected hermaphrodites (P0s) were singled and screened for Dumpy (Dpy) or Roller (Rol) offspring (F1s), both phenotypes associated with mutations in *dpy-10*. One hundred F1s were singled from a selected P0. Genotyping the F1s and their descendants (F2s) identified two strains homozygous for identical chromosomal deletions of precisely the 21 nucleotides comprising the LCS.

One *nhr-23(aaa20)* strain was backcrossed to N2 thrice prior to phenotypic analysis. No edits in the *dpy-10* gene were found in the backcrossed strain (ARF414).

Quantitative Fluorescence Microscopy

C. elegans were anesthetized with 2.5% NaN_3 (v/v) in M9 buffer, mounted on 2% agarose pads, and observed using a Zeiss Axioplan compound microscope with an attached Hamamatsu Orca ER CCD camera. The image acquisition and analysis software package Volocity 6.3 (Perkin Elmer) was used to control the microscope and digital camera and also to measure average fluorescence intensities within selected regions of interest (ROIs). In particular experiments, transgenic animals were staged partly by DIC microscopy and imaged during the L3/L4 or L4/A molts. Molting animals were identified by occlusion of the buccal cavity (Monsalve et al., 2011). Stereotypical rearrangements of vulva precursor cells (VPCs) demarcated early versus late sub-stages of the L3/L4 molt. The presence of a lumen in the incipient vulva demarcated early versus late sub-stages of the L4/A molt (Gupta et al., 2012; Van Buskirk and Sternberg, 2007).

To measure GFP signals associated with the *let-7p::nls-gfp* transcriptional reporter (Kai et al., 2013), worms were imaged at 400X total magnification. Both DIC and fluorescence images of the lateral epidermis were acquired – the latter with an exposure time of 25ms. Three nuclei in hyp7 and three in the seam were traced from the DIC image of each worm. The average fluorescence intensity within each nucleus was then measured and corrected for background signal. The average values for both hyp7 and seam nuclei (per worm) were used in further statistical analysis.

Signals associated with tdTomato and GFP expressed from bicistronic reporters for regulatory elements within 3′UTRs were measured using similar approaches. In this case, three distinct ROIs with areas of 40–70um^2 were manually selected per worm; each ROI included approximately equal areas of the nucleus and cytoplasm. In addition, multiple images of tdTomato and GFP were automatically captured over a range of exposure times. The average fluorescence intensity of each ROI was measured and plotted versus the exposure time. Values within the linear range of the assay were then used to determine the ratiometric signal (tdTomato/GFP) for each ROI. The average ratiometric value of all three ROIs per worm was used for subsequent statistical analysis. Notably, the morphology of the vulva was abnormal in a subset (≤ 10%) of

722 animals that expressed any bicistronic reporter. Because the phenotype precluded
723 staging by the abovementioned criteria, this subset of animals was excluded from the
724 analysis.
725
726 **Isolation of RNA**
727 RNA was extracted from developmentally synchronized *C. elegans* as described
728 (McCulloch and Rougvie, 2014). Using light microscopy, the fraction of pumping (active)
729 versus non-pumping (lethargic) animals in each sample was counted prior to collection
730 (n = 50-100). Troughs in the percentage of pumping animals were used to delimit
731 quiescent intervals *post-hoc.* Pellets containing ten to fifteen thousand worms (~100 µl)
732 were re-suspended in 4 volumes of TRIzol (ThermoFisher Scientific) and 1 volume of
733 glass beads 400-625 µm in diameter (Sigma). The suspensions were vortexed, flash
734 frozen, and thawed thrice. Samples were then mixed with 0.17 volumes of 24:1
735 chloroform: isoamyl alcohol (OmniPur) and centrifuged. The aqueous layer was
736 collected, mixed with an equal volume of 5:1 acid phenol: chloroform (ThermoFisher
737 Scientific), and centrifuged again. After collection of the top layer, RNA was extracted by
738 precipitation with ice-cold isopropanol (Sigma) and GlycoBlue (ThermoFisher Scientific).
739 The concentration of RNA in each time sample was measured using a NanoDrop 2000
740 (ThermoFisher Scientific). Thereafter, 5 µg of total RNA per sample was treated with 2U
741 of TURBO DNase (ThermoFisher Scientific) for 1 h. Notably, RNA samples used to
742 quantify mature *let-7* were not pre-treated with DNAse.
743
744 **Quantitative RT-PCR**
745 The sequences of gene-specific RT primers and identifiers for TaqMan assays
746 used in this research are provided in the Key Resources Table. To quantify levels of
747 primary *let-7* and *ama-1* transcripts in the abovementioned extracts, we processed 50ng
748 of RNA using a High-Capacity cDNA Reverse Transcription Kit (ThermoFisher
749 Scientific). Reaction mixtures of 15µL included random primers, dNTPs, RNaseOUT,
750 and reverse transcriptase, per the manufacturer's guidelines. To quantify levels of
751 mature *let-7* and the U18 small nucleolar (sno) RNA, we processed RNA with the same
752 kit but used gene-specific rather than random primers. Three volumes of nuclease-free
753 water were added to completed RT reactions. Next, we set-up TaqMan assays
754 (ThermoFisher Scientific) in 96-well plates, in triplicate. Per the manufacturer's

instructions, each reaction included TaqMan Universal PCR Master Mix, no AmpErase UNG, gene-specific primers, and 1.3μL of the preceding RT product in a volume of 20μL. Reactions ran on a Stratagene MX3000P (Agilent Genomics). To measure levels of protein-coding transcripts, 1μg of RNA was reverse transcribed using the enzyme Transcriptor (Roche). Each reaction mixture (20μL) also included hexadeoxynucleotide primers (Promega), dNTPs and RNasin (Promega). Four volumes of nuclease-free water were added to completed RT reactions. TaqMan assays were performed as described using 2μL of the RT product as template in a volume of 10μL.

The amount of template used in each TaqMan assay gave Ct values in the linear range of 21 to 36. In nearly all cases, technical replicates gave Ct values within 95% of the mean and the mean Ct value was used in subsequent analyses. Separate TaqMan reactions using templates made in the absence of reverse transcriptase produced no detectable PCR products, confirming the amplification of RNA rather than genomic DNA. As described, the levels of transcripts of interest were normalized to the levels of *ama-1* mRNAs or U18 snoRNAs within each sample, which were quantified in parallel TaqMan assays. For studies of gene expression over several developmental stages, the normalized values for each time sample were further standardized to the mean of all time samples derived from mock-treated or wild-type animals.

Bioinformatic Analyses

DNA sequences corresponding to the upstream regulatory region, first intron and 3′UTR for each nematode gene of interest were retrieved from WormBase (WS) v.264 and saved as SnapGene v.4 (GSL Biotech) files. The upstream sequences extracted from WS included all nucleotides between the transcriptional start site of the gene of interest and the nearest protein-coding gene. Particular sequences were extended or shortened based on gene models, ESTs and transcriptional start sites archived in WS264. If the gene of interest lacked an annotated 3′UTR, then we initially retrieved 1 kb of sequence downstream of the stop codon. Particular 3′UTR sequences were revised based on ESTs and poly-AAA sites that are archived in WS264 but not yet incorporated in current gene models.

Both the upstream regulatory regions of vertebrate homologs of *let-7* and the 3′UTRs of vertebrate homologs of *nhr-23*/*RORs* were retrieved from the UCSC genome browser. Three human genes, two mouse genes, and six zebrafish genes encode

mature miRNAs identical in sequence to *C. elegans let-7*. We extracted 3 kb of sequence upstream of each *let-7* homolog, except in the case of *H. sapiens let-7a-3*, wherein the core promoter has been experimentally delimited to 1 kb of upstream sequence (Wang et al., 2012). For a given gene, the longest 3′UTR was selected if multiple 3′UTRs existed. The 3′UTR sequences were individually and systematically validated by comparison with EST; only those genes with annotated 3′UTRs supported by ESTs were included in further analyses.

To identify ROR response elements that might function as transcriptional enhancers of miRNAs or protein-coding genes of interest, we searched the upstream regulatory sequences and/or first introns for instances of the consensus response element 5′-(A/G)GGTCA-3′ on both the coding and anti-coding strands of DNA. Figure 1A and Supplemental Figures 1A and 4A depict the results of these computational searches. To accurately calculate the probability of an RORE occurring by chance, we first used the k-mer counting software program DSK (Rizk G. et al, 2013) to determine that the reference genome of *C. elegans*, which comprises 100.2 mega bases, includes 41,203 distinct instances of the consensus RORE. For non-nematodes, the expected frequency was the chance of either six-nucleotide sequence appearing in a longer oligonucleotide; this frequency is approximately one per 1 kb.

Regions of *C. elegans* chromosomal DNA occupied by NHR-23 *in vivo* were identified on the modEncode *C. elegans* Genome Browser (v. 2.48). The two relevant datasets archived therein were Chip-Seq of strain OP43 cultivated at 20°C and harvested during the L2 or L3 stage. Most ID in L3, addition in L2. Both used – not discriminate the two here. The upstream regulatory sequences and/or first intron for each gene of interest were viewed in this browser. Regions of significant enrichment (“peaks”) were identified by z-scores ≥ 2 (Celniker et al., 2009). Sequences extracted and aligned with the upstream regulatory regions and/or first intron as above, adjusting for differences in the related chromosomal coordinates between WS220 and WS264.

Evidence of direct or indirect regulation of transcript levels by NHR-23 was either detected by Affymetrix microarrays in 2-3/3 biological replicates (Kouns et al., 2011), or shown prior publications (*lin-42a/b*, *nas-36*). Expression was at least 1.2-fold lower in *nhr-23* knockdowns than mock-treated larvae.

Targets of NHR-23 followed 2 out of the 3 following criteria: 1) The upstream regulatory region and/or first intron contained Chip-Seq NHR-23 peaks (Celniker et al.,

2009); 2) the same region contained more ROREs than predicted by chance alone; and 3) Expression was 1.2-fold lower in *nhr-23* knockdowns than mock-treated larvae.

The software RNAhybrid (Rehmsmeier et al., 2004) was used to detect sequences partially complementary to the 21-nt. mature *let-7* in the 3′UTRs of annotated homologs of *nhr-23* in the genomes of *H. sapiens*, *M. musculus*, *D. rerio* and *C. briggsae*. Mature *C. elegans let-7*, which is identical to human *let-7*a, was used as the query sequence. No more than 1 mismatched nucleotide within the *let-7* seed sequence was tolerated for the prediction of LCSs in this report.

Targets of *let-7* fulfilled both of the following criteria: 1) LCSs, with up to one mismatch in the seed region, were detected in the 3′UTR more often than, or equal to, the number predicted by chance alone (Rehmsmeier et al., 2004); and (2) ALG-1 co-IP the 3′UTR, on the coding strand of the gene by iCLIP-Seq (Broughton et al., 2016).

Genes were determined to be “involved in molting” based on the literature. For example, if mutations in a particular gene caused a molting defective phenotype, the gene was considered to be involved in molting (Frand et al., 2005). Similarly, if inactivation of the gene had an effect on lethargus, the gene was also considered to be involved in the molting cycle.

Genes were annotated as “oscillatory” based on published RNA-Seq studies (Hendriks et al., 2014; Kim et al., 2013); therein, genes whose expression at 8-10 h intervals was significantly correlated ($P<0.05$) were considered to be cycling in expression.

QUANTIFICATION AND STATISTICAL ANALYSIS

The software package Volocity 6.3 (Perkin Elmer) was used to BOTH acquire fluorescence micrographs and measure the signal intensity of selected ROIs. The software package GraphPad Prism v6.0h was used for all statistical tests. Samples sizes for all experiments, statistical analysis, and outcomes thereof are specified in each figure and/or corresponding legend.

SUPPLEMENTAL FIGURE LEGENDS

Supplemental Figure 1. NHR-23 activates pulsatile expression of the *lin-42* gene. **A)** Schematic shows the correspondence among annotated regulatory regions of seven *lin-42* variants (WS264) and ten chromosomal regions occupied by NHR-23 in mid-stage larvae. Dashed lines demarcate defined promoters; arrows label transcriptional start sites. Coordinates refer to *C. elegans* Chr. II (NC_003280). **B)** Relative levels of *lin-42* transcripts detected in *nhr-23(RNAi)* versus mock-treated animals by TaqMan qRT-PCR. Each value was first normalized to *ama-1* transcript levels in the same sample. All values were then normalized to the mean of all mock-treated time samples. Symbols represent the mean and range from two biological replicates. The x-axis indicates time elapsed (h) on food. Bars beneath the x-axis depict progression of the life cycle; gray boxes therein signify observed intervals of quiescence. The times of initial exposure to *nhr-23* siRNAs and the appearance of molting-defective *nhr-23(RNAi)* larvae are indicated.

Supplemental Figure 2. Proposed molecular mechanism for the bicistronic reporter system. Schematic depicts expression from the *dpy-7* promoter and trans-splicing followed by standalone translation of tdTomato and GFP. (Left) Equimolar levels of tdTomato and GFP in the absence of 3′UTR-mediated repression. To predict the resulting ratiometric signal, the synthesis and degradation of transcripts and proteins were considered equally efficient. If so, then a ratiometric signal of 2.4 was expected, based on the brightness of tdTomato and GFP, respectively, 95 and 39 $(mM \bullet cm)^{-1}$ (Shaner et al., 2005). (Right) Anticipated events for a 3'UTR targeted by a miRNA. The illustration depicts *let-7*, specifically, because the test 3'UTRs all contained complementary sites. concept

Supplemental Figure 3. The LCS mediates repression of *nhr-23* from late L2 through young adulthood. A-A′) Normalized levels of *nhr-23* transcripts detected by TaqMan qRT-PCR in regular 2 h time samples of *let-7(n2853)*, *nhr-23(aaa20)* and wild-type animals. Values obtained from an independent trial are presented as per Figure 4A. Note that these time samples include a relatively small fraction of the adult stage. All three samples were collected after 24-50 h on food. **B)** As above, for *nhr-23*

882 transcripts detected in *mir-41(Δ) mir-241(Δ); mir-84(n4037)* triple mutants,
883 *nhr-23(aaa20)* single mutants, and wild-type larvae progressing from late L1 through
884 mid L3. Both the *let-7s* triple knockout and wild-type larvae were collected 14–26 h after
885 release from starvation; *nhr-23(aaa20)* larvae, 16–28 h after release.
886
887 **Supplemental Figure 4. Reciprocal target sequences for RORs and *let*-7-family**
888 **miRNAs identified in vertebrates. A)** Schematics show ROREs (brown), upstream
889 regulatory sequences (gray), and homologs of mature *let-7* (pink) found in annotated
890 genomes of the indicated species. Arrows are aesthetic landmarks for as-yet undefined
891 transcriptional start sites. B) Schematics show LCSs (gold), 3′UTRs (blue), and stop
892 codons (black) of annotated *ROR* homologs. Gradients and bold labels distinguish sites
893 perfectly complementary to the seed of *let-7s*. The selected 3′UTRs were retrieved from
894 the UCSC genome browser; verified by curated ESTs; and searched using RNAhybrid.
895 Supplemental Table 2 includes more information about the depicted LCSs.
896
897 **Supplemental Table 1. Comparative Metrics of Molting Biorhythms.**
898 Chart includes the average duration (h) of active and lethargic intervals, and also the
899 wake-to-wake interval, for cohorts of *nhr-23(RNAi)*, *let-7*-family mutants and wild-type
900 animals progressing through the indicated stages. ****p<0.0001, ***p≤0.001, *p≤0.05 for
901 pairwise comparisons with age-matched, mock-treated wild-type cohorts; Ordinary One-
902 Way ANOVA with Bonferroni's correction for multiple comparisons. All animals were
903 cultivated on *E. coli* HT115(DE3) transformed by empty vector unless otherwise
904 specified.
905
906 **Supplemental Table 2. LCSs found in nematode and vertebrate homologs of *ROR*.**
907 Entries correspond to sites shown in Supplemental Figure 4B. The number of nt.
908 between the 3′ end of each LCS and the stop codon is specified. Thermostability values
909 for RNA duplexes between mature *let-7* and each LCS were predicted using
910 RNAhybrid**.** The predicted values for all entries are lower than predicted thermostability
911 of duplexes between *let-7* and its target site in the 3′UTR of *lin-41,* which is -29 kcal/mol
912 (Rehmsmeier et al., 2004)
913

Supplemental Table 3. Classification of genes linked to molting as targets of NHR-23, *let*-7s, neither or both. The bioinformatic approaches and criteria for assignment of queries to categories are described in the detailed methods. The name and WormBase accession number of each gene is listed. The value of "# Obs/# Exp" in column 5 indicates the ratio of the number of ROREs observed to the number expected by chance alone, as described in the Methods. Genes that were detected as down regulated in *nhr-23(RNAi)* animals, relative to controls, using microarray analysis or other techniques, are indicated as "⬇" in column 6. A "Y" in column 7 indicates that the gene was considered a target of NHR-23. The value of "# Obs/# Exp" in column 11 indicates the ratio of the number of LCSs observed to the number expected by chance alone, as described in the Methods. Genes with 3′UTRs bound by ALG-1 are indicated by a "+" symbol in column 12. A "Y" in column 13 indicates that a particular gene was considered a target of let-7. A "〰" in column 15 indicates that expression of the gene oscillates throughout development.

REFERENCES

Abbott, A.L., Alvarez-Saavedra, E., Miska, E.A., Lau, N.C., Bartel, D.P., Horvitz, H.R., and Ambros, V. (2005). The let-7 MicroRNA family members mir-48, mir-84, and mir-241 function together to regulate developmental timing in Caenorhabditis elegans. Dev Cell *9*, 403-414.

Ambros, V., and Ruvkun, G. (2018). Recent Molecular Genetic Explorations of Caenorhabditis elegans MicroRNAs. Genetics *209*, 651-673.

Antebi, A. (2015). Nuclear receptor signal transduction in C. elegans. WormBook, 1-49.

Bethke, A., Fielenbach, N., Wang, Z., Mangelsdorf, D.J., and Antebi, A. (2009). Nuclear hormone receptor regulation of microRNAs controls developmental progression. Science *324*, 95-98.

Bracht, J., Hunter, S., Eachus, R., Weeks, P., and Pasquinelli, A.E. (2004). Trans-splicing and polyadenylation of let-7 microRNA primary transcripts. RNA *10*, 1586-1594.

Broughton, J.P., Lovci, M.T., Huang, J.L., Yeo, G.W., and Pasquinelli, A.E. (2016). Pairing beyond the Seed Supports MicroRNA Targeting Specificity. Mol Cell *64*, 320-333.

Celniker, S.E., Dillon, L.A., Gerstein, M.B., Gunsalus, K.C., Henikoff, S., Karpen, G.H., Kellis, M., Lai, E.C., Lieb, J.D., MacAlpine, D.M.*, et al.* (2009). Unlocking the secrets of the genome. Nature *459*, 927-930.

Chen, D., Taylor, K.P., Hall, Q., and Kaplan, J.M. (2016). The Neuropeptides FLP-2 and PDF-1 Act in Concert To Arouse Caenorhabditis elegans Locomotion. Genetics *204*, 1151-1159.

Cook, D.N., Kang, H.S., and Jetten, A.M. (2015). Retinoic Acid-Related Orphan Receptors (RORs): Regulatory Functions in Immunity, Development, Circadian Rhythm, and Metabolism. Nucl Receptor Res *2*.

Driver, R.J., Lamb, A.L., Wyner, A.J., and Raizen, D.M. (2013). DAF-16/FOXO regulates homeostasis of essential sleep-like behavior during larval transitions in C. elegans. Curr Biol *23*, 501-506.

Ecsedi, M., Rausch, M., and Grosshans, H. (2015). The let-7 microRNA directs vulval development through a single target. Dev Cell *32*, 335-344.

Edelman, T.L., McCulloch, K.A., Barr, A., Frokjaer-Jensen, C., Jorgensen, E.M., and Rougvie, A.E. (2016). Analysis of a lin-42/Period Null Allele Implicates All Three Isoforms in Regulation of Caenorhabditis elegans Molting and Developmental Timing. G3 (Bethesda).

El-Sherif, E., Averof, M., and Brown, S.J. (2012). A segmentation clock operating in blastoderm and germband stages of Tribolium development. Development *139*, 4341-4346.

Frand, A.R., Russel, S., and Ruvkun, G. (2005). Functional genomic analysis of C. elegans molting. PLoS Biol *3*, e312.

Galles, C., Prez, G.M., Penkov, S., Boland, S., Porta, E.O.J., Altabe, S.G., Labadie, G.R., Schmidt, U., Knolker, H.J., Kurzchalia, T.V.*, et al.* (2018). Endocannabinoids in Caenorhabditis elegans are essential for the mobilization of cholesterol from internal reserves. Sci Rep *8*, 6398.

Gomez, C., Ozbudak, E.M., Wunderlich, J., Baumann, D., Lewis, J., and Pourquie, O. (2008). Control of segment number in vertebrate embryos. Nature *454*, 335-339.

Gupta, B.P., Hanna-Rose, W., and Sternberg, P.W. (2012). Morphogenesis of the vulva and the vulval-uterine connection. WormBook, 1-20.

Hammell, C.M., Karp, X., and Ambros, V. (2009). A feedback circuit involving let-7-family miRNAs and DAF-12 integrates environmental signals and developmental timing in Caenorhabditis elegans. Proc Natl Acad Sci U S A *106*, 18668-18673.

Hayes, G.D., Frand, A.R., and Ruvkun, G. (2006). The mir-84 and let-7 paralogous microRNA genes of Caenorhabditis elegans direct the cessation of molting via the conserved nuclear hormone receptors NHR-23 and NHR-25. Development *133*, 4631-4641.

Hendriks, G.J., Gaidatzis, D., Aeschimann, F., and Grosshans, H. (2014). Extensive oscillatory gene expression during C. elegans larval development. Mol Cell *53*, 380-392.

Isik, M., Blackwell, T.K., and Berezikov, E. (2016). MicroRNA mir-34 provides robustness to environmental stress response via the DAF-16 network in C. elegans. Sci Rep *6*, 36766.

Iwanir, S., Tramm, N., Nagy, S., Wright, C., Ish, D., and Biron, D. (2013). The microarchitecture of C. elegans behavior during lethargus: homeostatic bout dynamics, a typical body posture, and regulation by a central neuron. Sleep *36*, 385-395.

Jeon, M., Gardner, H.F., Miller, E.A., Deshler, J., and Rougvie, A.E. (1999). Similarity of the C. elegans developmental timing protein LIN-42 to circadian rhythm proteins. Science *286*, 1141-1146.

Johnson, S.M., Lin, S.Y., and Slack, F.J. (2003). The time of appearance of the C. elegans let-7 microRNA is transcriptionally controlled utilizing a temporal regulatory element in its promoter. Dev Biol *259*, 364-379.

Kai, Z.S., Finnegan, E.F., Huang, S., and Pasquinelli, A.E. (2013). Multiple cis-elements and trans-acting factors regulate dynamic spatio-temporal transcription of let-7 in Caenorhabditis elegans. Dev Biol *374*, 223-233.

Kamath, R.S., Fraser, A.G., Dong, Y., Poulin, G., Durbin, R., Gotta, M., Kanapin, A., Le Bot, N., Moreno, S., Sohrmann, M.*, et al.* (2003). Systematic functional analysis of the Caenorhabditis elegans genome using RNAi. Nature *421*, 231-237.

Kim, D., Grun, D., and van Oudenaarden, A. (2013). Dampening of expression oscillations by synchronous regulation of a microRNA and its target. Nat Genet *45*, 1337-1344.

Kostrouchova, M., Krause, M., Kostrouch, Z., and Rall, J.E. (1998). CHR3: a Caenorhabditis elegans orphan nuclear hormone receptor required for proper epidermal development and molting. Development *125*, 1617-1626.

Kouns, N.A., Nakielna, J., Behensky, F., Krause, M.W., Kostrouch, Z., and Kostrouchova, M. (2011). NHR-23 dependent collagen and hedgehog-related genes required for molting. Biochem Biophys Res Commun *413*, 515-520.

Matsu-Ura, T., Dovzhenok, A., Aihara, E., Rood, J., Le, H., Ren, Y., Rosselot, A.E., Zhang, T., Lee, C., Obrietan, K.*, et al.* (2016). Intercellular Coupling of the Cell Cycle and Circadian Clock in Adult Stem Cell Culture. Mol Cell *64*, 900-912.

McCulloch, K.A., and Rougvie, A.E. (2014). Caenorhabditis elegans period homolog lin-42 regulates the timing of heterochronic miRNA expression. Proc Natl Acad Sci U S A *111*, 15450-15455.

Meli, V.S., Osuna, B., Ruvkun, G., and Frand, A.R. (2010). MLT-10 defines a family of DUF644 and proline-rich repeat proteins involved in the molting cycle of Caenorhabditis elegans. Mol Biol Cell *21*, 1648-1661.

Monsalve, G.C., Van Buskirk, C., and Frand, A.R. (2011). LIN-42/PERIOD controls cyclical and developmental progression of C. elegans molts. Curr Biol *21*, 2033-2045.

Nelson, M.D., Lee, K.H., Churgin, M.A., Hill, A.J., Van Buskirk, C., Fang-Yen, C., and Raizen, D.M. (2014). FMRFamide-like FLP-13 neuropeptides promote quiescence following heat stress in Caenorhabditis elegans. Curr Biol *24*, 2406-2410.

Olmedo, M., Merrow, M., and Geibel, M. (2017). Sleeping Beauty? Developmental Timing, Sleep, and the Circadian Clock in Caenorhabditis elegans. Adv Genet *97*, 43-80.

Paix, A., Folkmann, A., Rasoloson, D., and Seydoux, G. (2015). High Efficiency, Homology-Directed Genome Editing in Caenorhabditis elegans Using CRISPR-Cas9 Ribonucleoprotein Complexes. Genetics *201*, 47-54.

Perales, R., King, D.M., Aguirre-Chen, C., and Hammell, C.M. (2014). LIN-42, the Caenorhabditis elegans PERIOD homolog, negatively regulates microRNA transcription. PLoS Genet *10*, e1004486.

Raizen, D.M., Zimmerman, J.E., Maycock, M.H., Ta, U.D., You, Y.J., Sundaram, M.V., and Pack, A.I. (2008). Lethargus is a Caenorhabditis elegans sleep-like state. Nature *451*, 569-572.

Rehmsmeier, M., Steffen, P., Hochsmann, M., and Giegerich, R. (2004). Fast and effective prediction of microRNA/target duplexes. RNA *10*, 1507-1517.

Reinhart, B.J., Slack, F.J., Basson, M., Pasquinelli, A.E., Bettinger, J.C., Rougvie, A.E., Horvitz, H.R., and Ruvkun, G. (2000). The 21-nucleotide let-7 RNA regulates developmental timing in Caenorhabditis elegans. Nature *403*, 901-906.

Santori, F.R., Huang, P., van de Pavert, S.A., Douglass, E.F., Jr., Leaver, D.J., Haubrich, B.A., Keber, R., Lorbek, G., Konijn, T., Rosales, B.N.*, et al.* (2015). Identification of natural RORgamma ligands that regulate the development of lymphoid cells. Cell Metab *21*, 286-298.

Shaner, N.C., Steinbach, P.A., and Tsien, R.Y. (2005). A guide to choosing fluorescent proteins. Nat Methods *2*, 905-909.

Singh, K., Chao, M.Y., Somers, G.A., Komatsu, H., Corkins, M.E., Larkins-Ford, J., Tucey, T., Dionne, H.M., Walsh, M.B., Beaumont, E.K.*, et al.* (2011). C. elegans Notch signaling regulates adult chemosensory response and larval molting quiescence. Curr Biol *21*, 825-834.

Singh, R.N., and Sulston, J.E. (1978). Some observations on moulting in Caenorhabditis elegans. Nematologica *24*, 63-71.

Sparrow, D.B., Chapman, G., Turnpenny, P.D., and Dunwoodie, S.L. (2007). Disruption of the somitic molecular clock causes abnormal vertebral segmentation. Birth Defects Res C Embryo Today *81*, 93-110.

Stiernagle, T. (2006). Maintenance of C. elegans. WormBook, 1-11.

Takahashi, J.S. (2016). Molecular Architecture of the Circadian Clock in Mammals. In A Time for Metabolism and Hormones, P. Sassone-Corsi, and Y. Christen, eds. (Cham (CH)), pp. 13-24.

Takahashi, J.S. (2017). Transcriptional architecture of the mammalian circadian clock. Nat Rev Genet *18*, 164-179.

Timmons, L., Court, D.L., and Fire, A. (2001). Ingestion of bacterially expressed dsRNAs can produce specific and potent genetic interference in Caenorhabditis elegans. Gene *263*, 103-112.

Trojanowski, N.F., and Raizen, D.M. (2016). Call it Worm Sleep. Trends Neurosci *39*, 54-62.

Ueda, H.R., Chen, W., Adachi, A., Wakamatsu, H., Hayashi, S., Takasugi, T., Nagano, M., Nakahama, K., Suzuki, Y., Sugano, S.*, et al.* (2002). A transcription factor response element for gene expression during circadian night. Nature *418*, 534-539.

Van Buskirk, C., and Sternberg, P.W. (2007). Epidermal growth factor signaling induces behavioral quiescence in Caenorhabditis elegans. Nat Neurosci *10*, 1300-1307.

Van Wynsberghe, P.M., Finnegan, E.F., Stark, T., Angelus, E.P., Homan, K.E., Yeo, G.W., and Pasquinelli, A.E. (2014). The Period protein homolog LIN-42 negatively regulates microRNA biogenesis in C. elegans. Dev Biol *390*, 126-135.

Van Wynsberghe, P.M., Kai, Z.S., Massirer, K.B., Burton, V.H., Yeo, G.W., and Pasquinelli, A.E. (2011). LIN-28 co-transcriptionally binds primary let-7 to regulate miRNA maturation in Caenorhabditis elegans. Nat Struct Mol Biol *18*, 302-308.

Vella, M.C., Choi, E.Y., Lin, S.Y., Reinert, K., and Slack, F.J. (2004). The C. elegans microRNA let-7 binds to imperfect let-7 complementary sites from the lin-41 3'UTR. Genes Dev *18*, 132-137.

Wang, D.J., Legesse-Miller, A., Johnson, E.L., and Coller, H.A. (2012). Regulation of the let-7a-3 promoter by NF-kappaB. PLoS One *7*, e31240.

Zhang, Y., Papazyan, R., Damle, M., Fang, B., Jager, J., Feng, D., Peed, L.C., Guan, D., Sun, Z., and Lazar, M.A. (2017). The hepatic circadian clock fine-tunes the lipogenic response to feeding through RORalpha/gamma. Genes Dev.

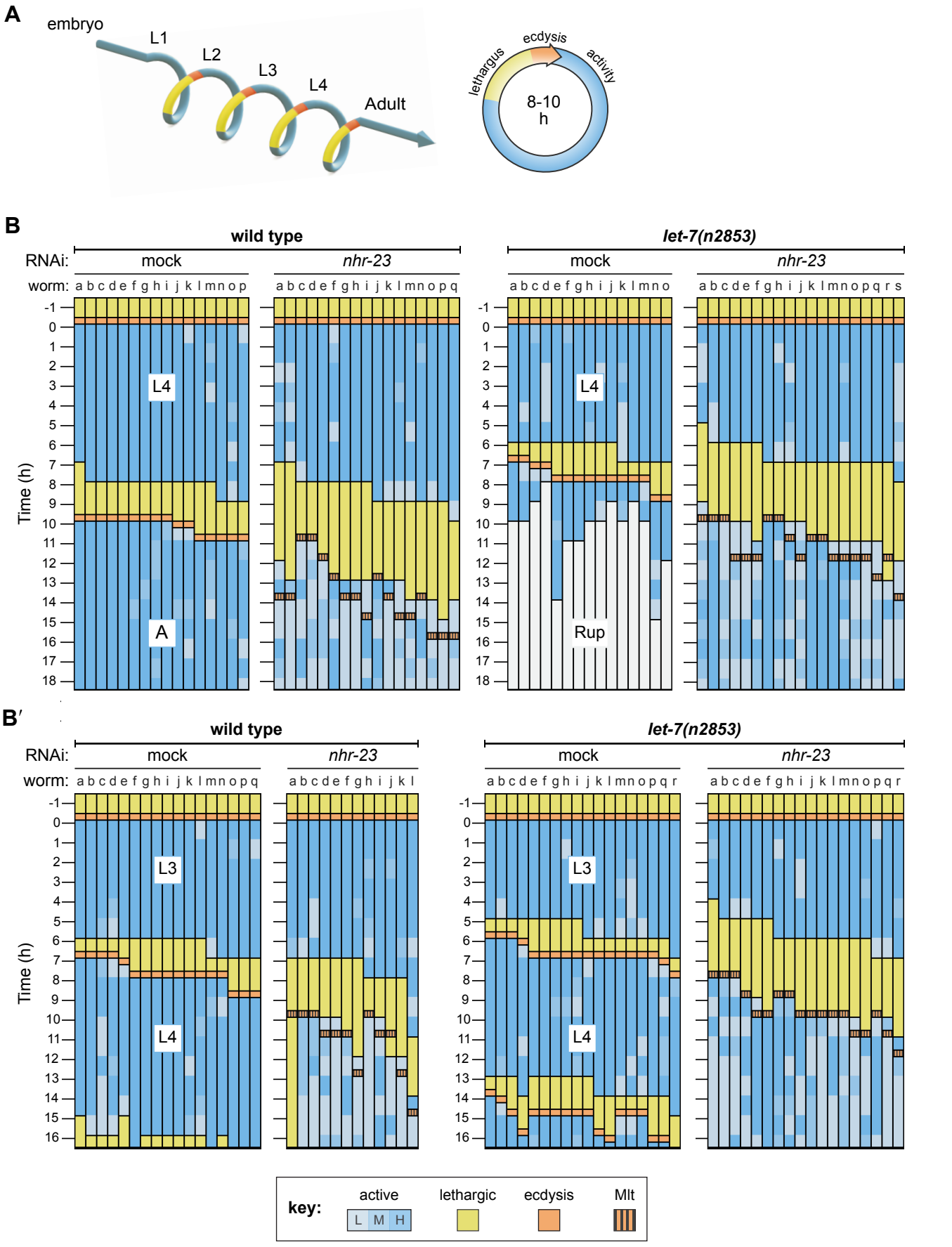

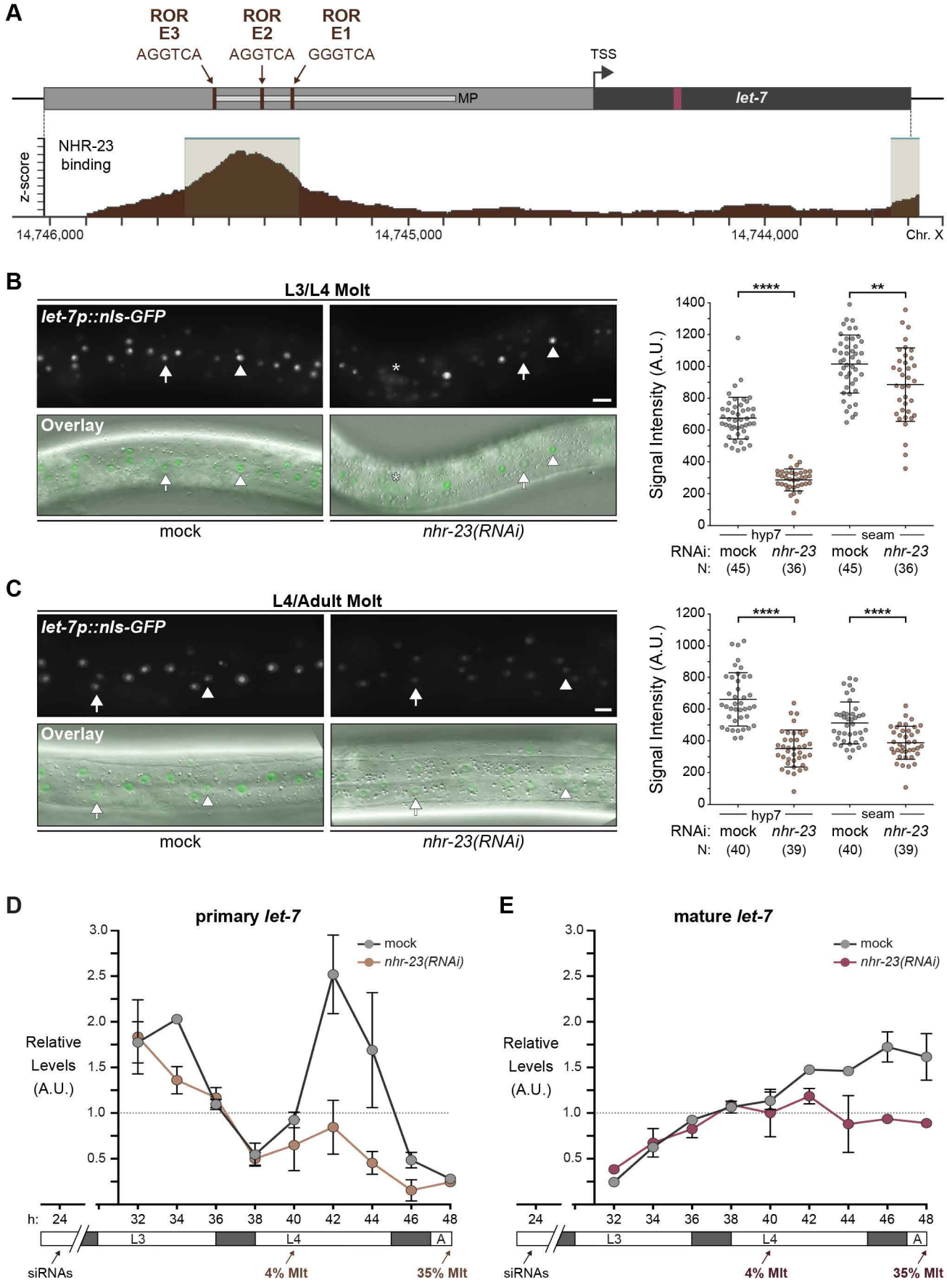

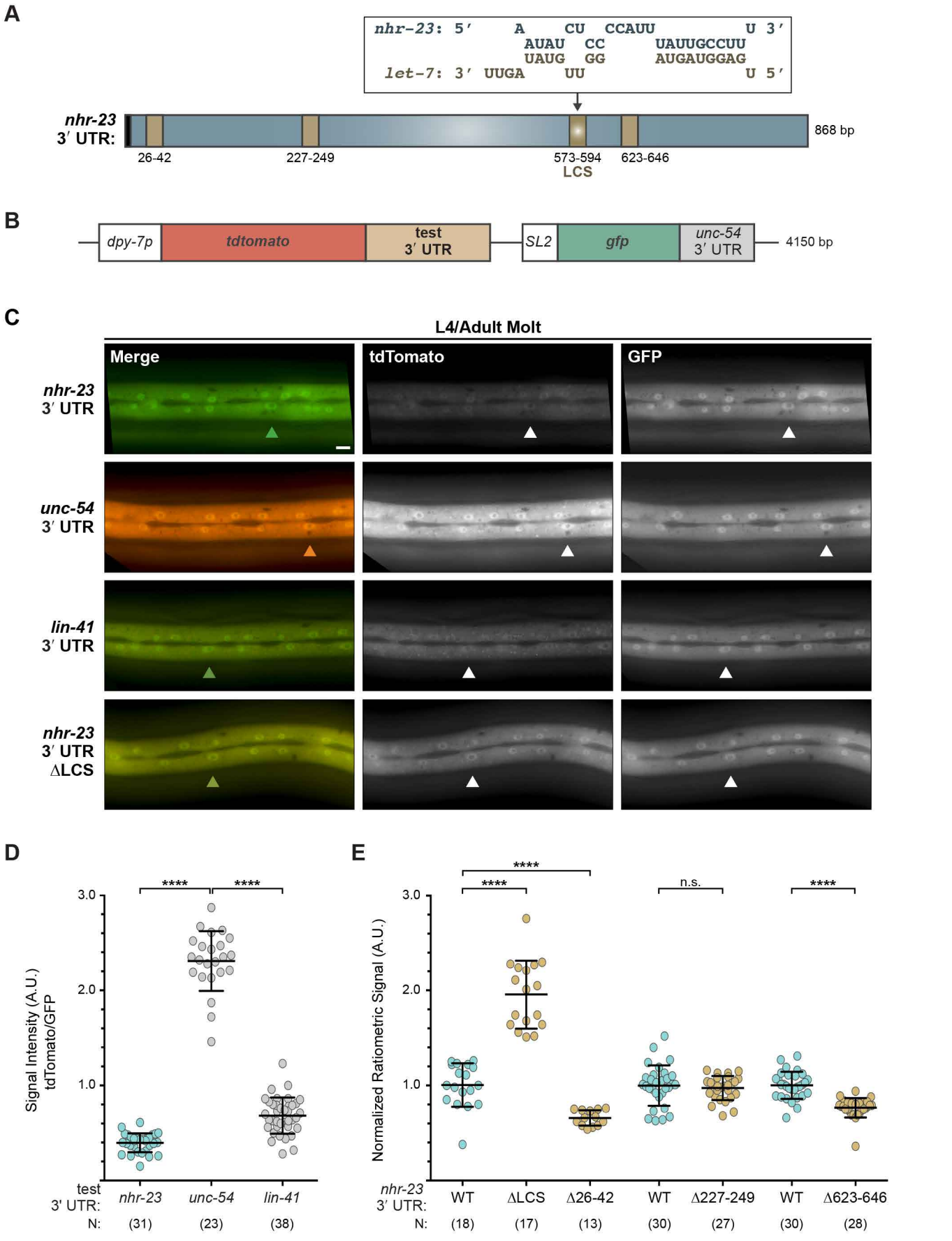

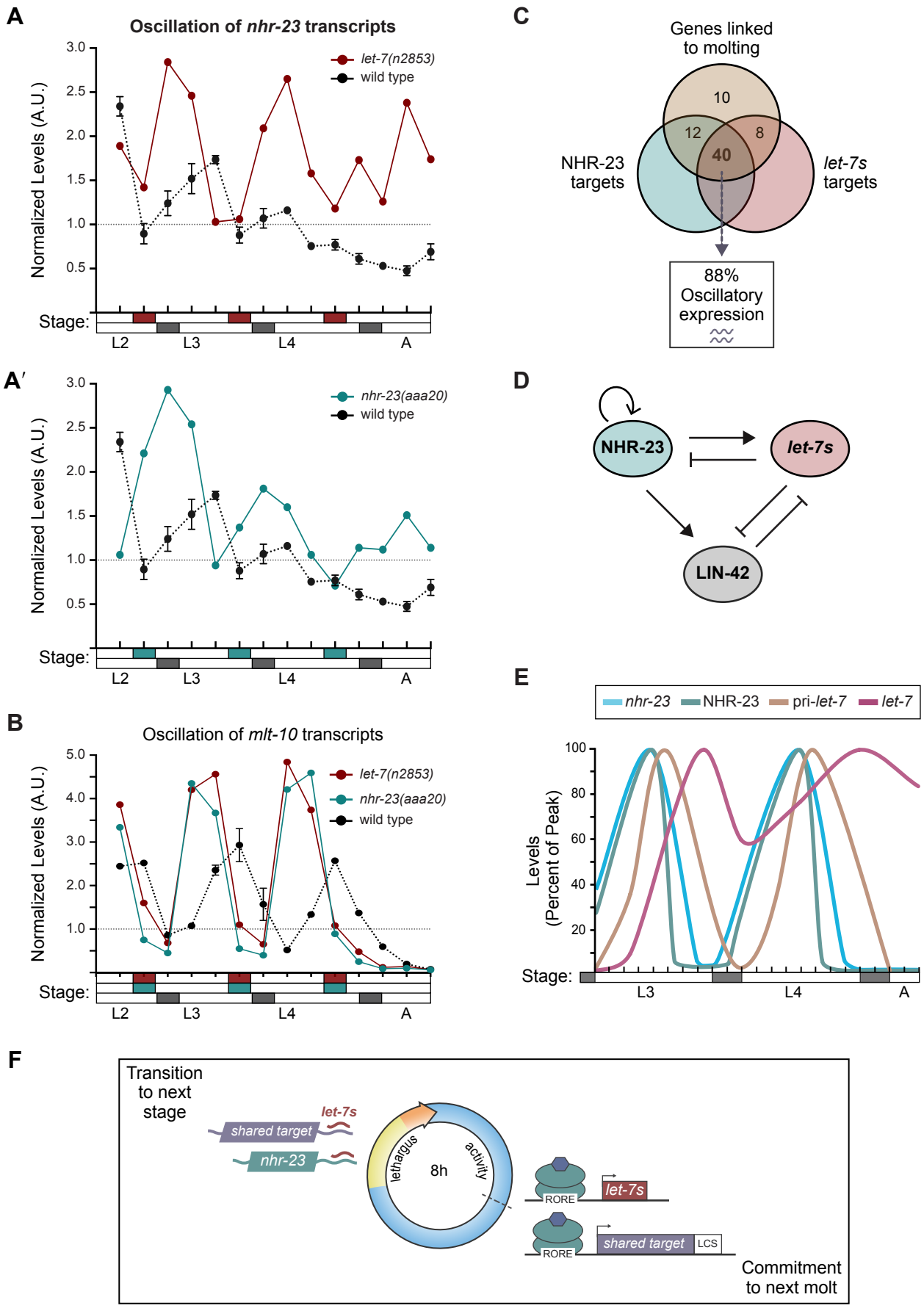

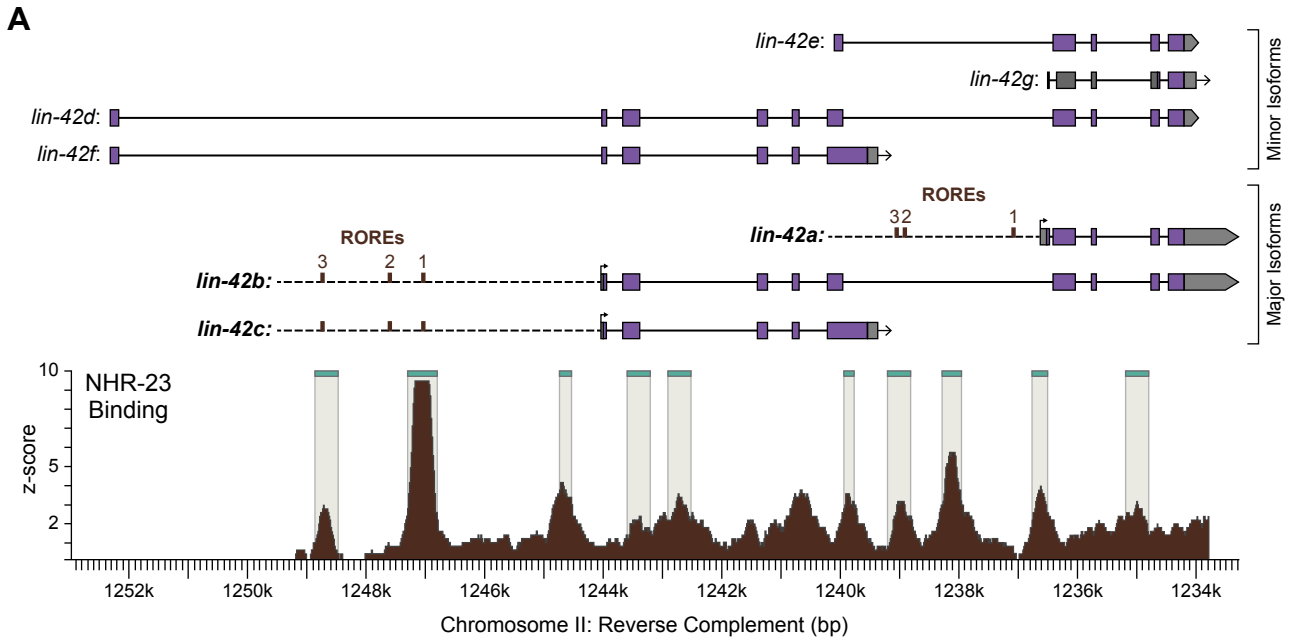

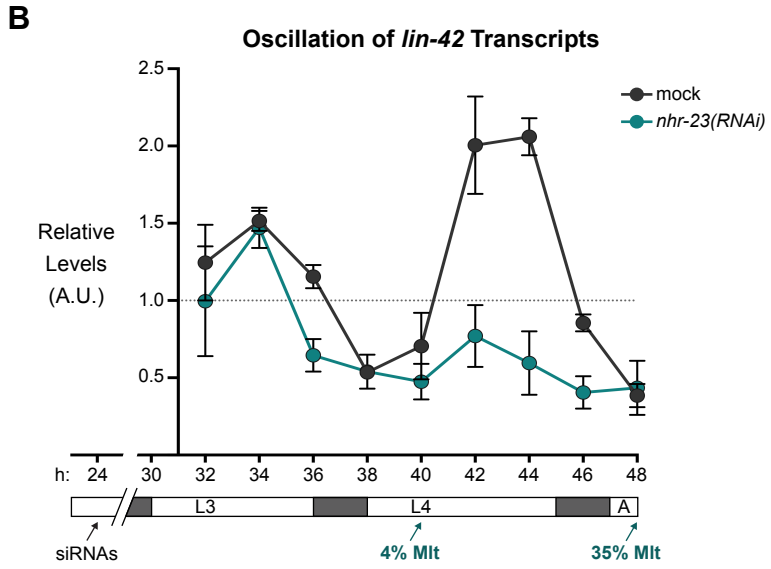

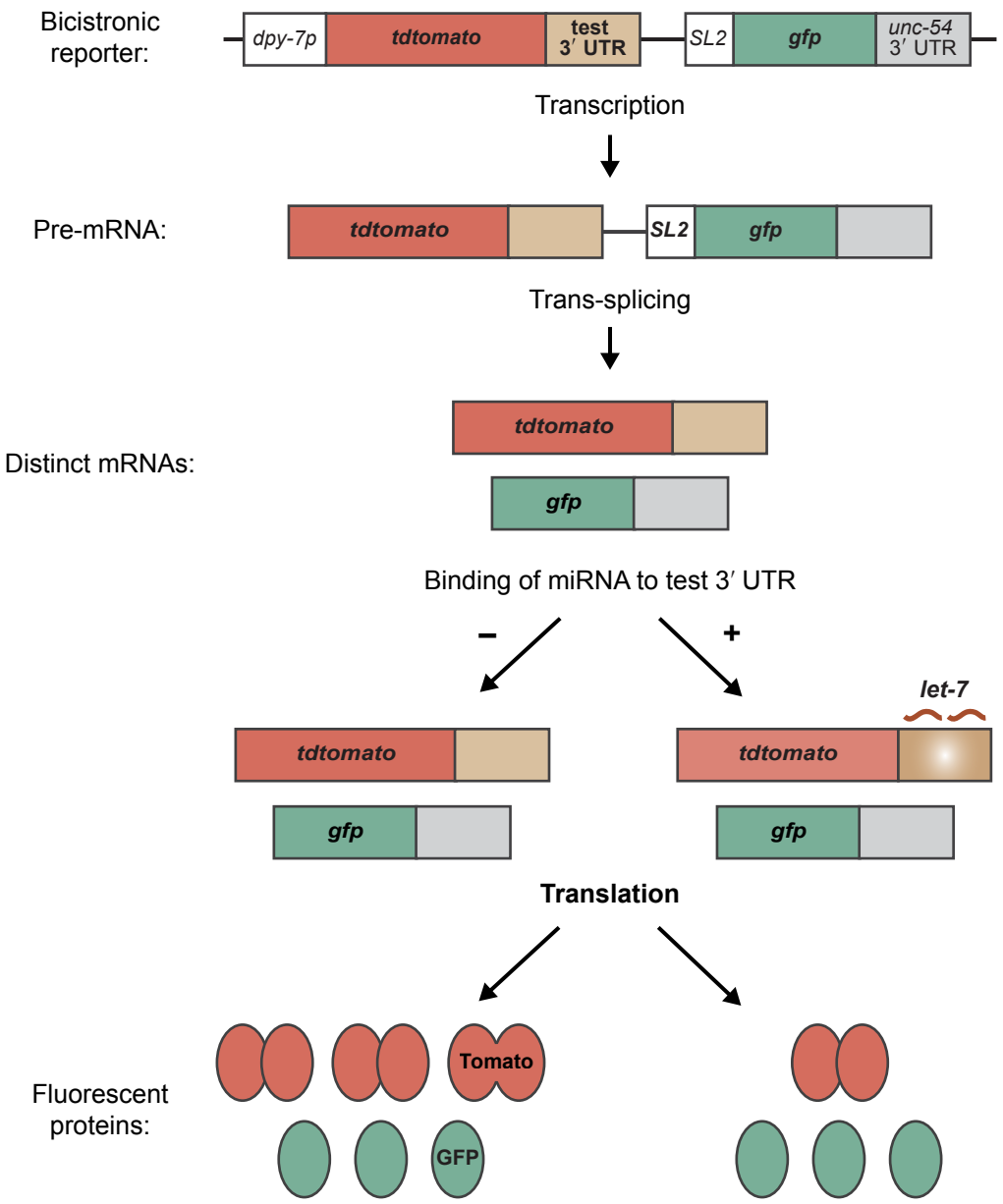

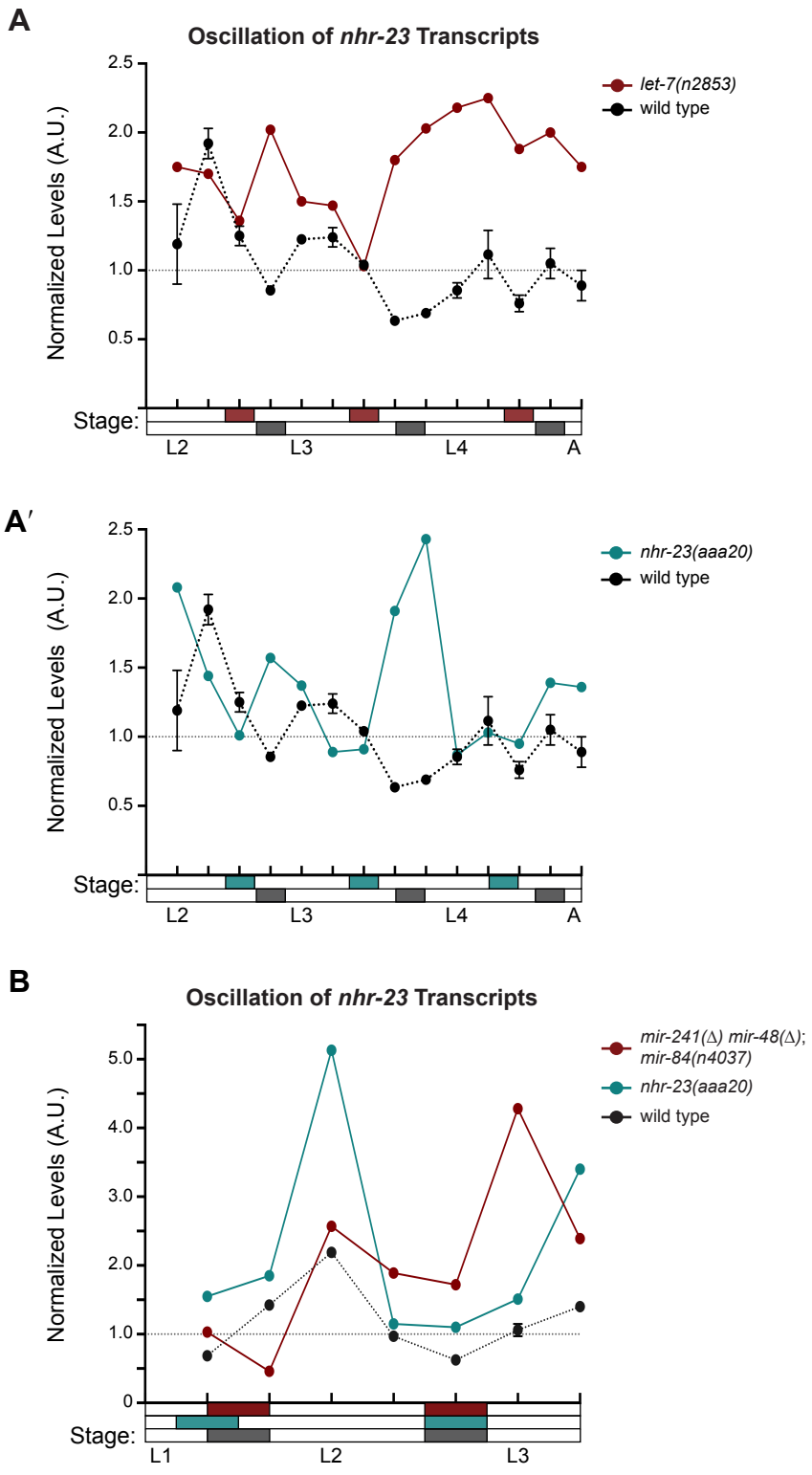

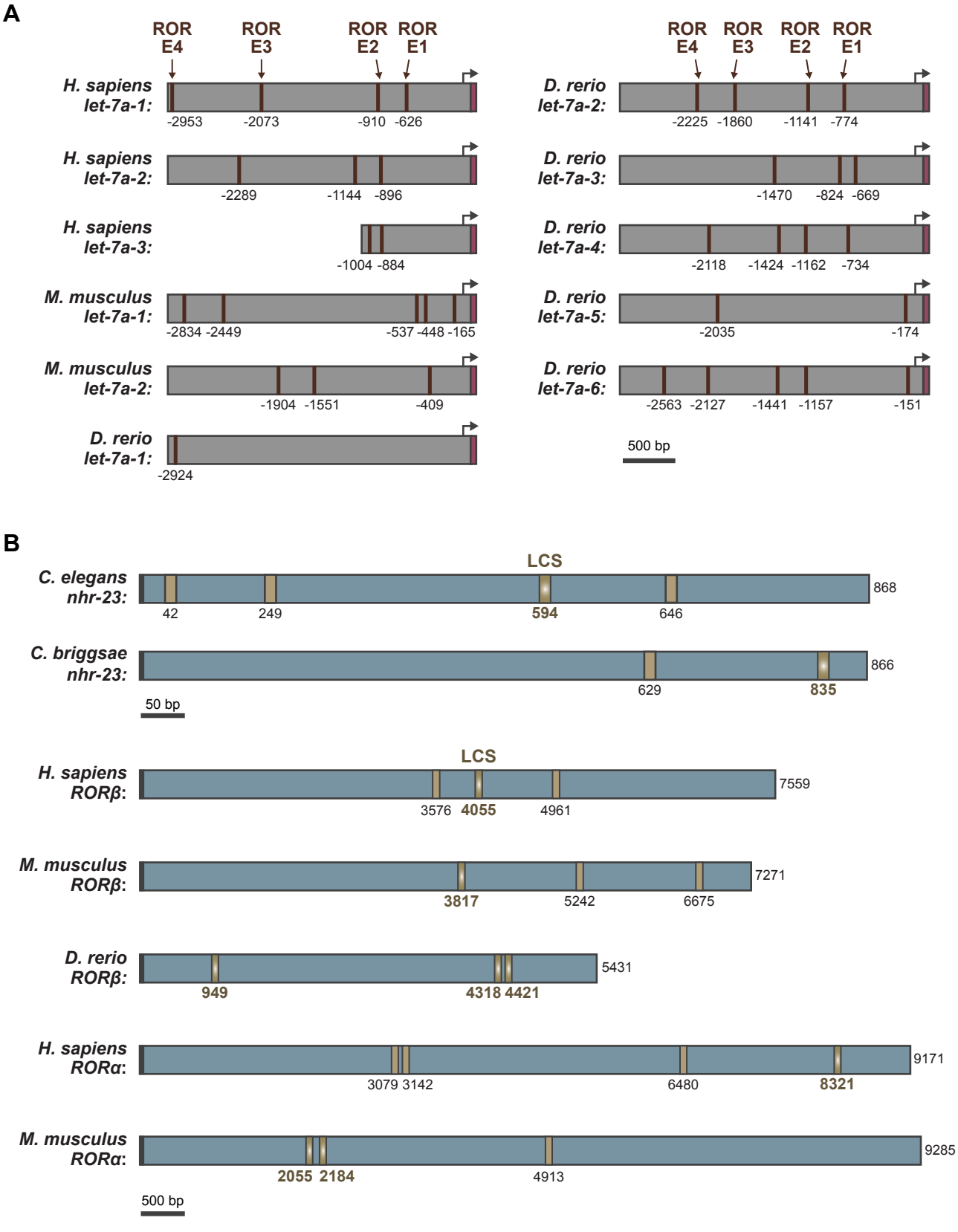

Supplemental Table 1 – Relates to Figure 1. Comparative Metrics of Molting Biorhythms

		Interval (h)												
		Active				Lethargic				Wake-to-Wake				
L2 to L3														
RNAi	**Strain**	mean	sd	cv	p	mean	sd	cv	p	mean	sd	cv	n	p
–	wild type	5.9	0.3	0.05	–	1.3	0.5	0.36	–	7.2	0.4	0.06	18	–
nhr-23	wild type	6.1	0.6	0.10	n.s.	3.9	1.1	0.28	****	9.9	1.0	0.10	19	****
–	*mir-41Δ mir-241Δ; mir-84(n4037)*	6.3	0.7	0.11	n.s.	1.3	0.5	0.36	n.s.	7.6	0.7	0.10	17	n.s.
nhr-23	*mir-41Δ mir-241Δ; mir-84(n4037)*	6.4	0.8	0.13	n.s.	3.0	0.4	0.13	****	9.4	0.8	0.09	15	****
L3 to L4														
RNAi	**Strain**	mean	sd	cv	p	mean	sd	cv	p	mean	sd	cv	n	p
–	wild type	6.3	0.4	0.07	–	1.6	0.5	0.31	–	7.9	0.7	0.08	17	–
nhr-23	wild type	7.7	1.2	0.15	****	3.8	1.9	0.49	****	11.4	1.9	0.16	12	****
–	*let-7(n2853)*†	5.6	0.6	0.11	*	1.3	0.4	0.36	n.s.	6.8	0.5	0.07	18	*
nhr-23	*let-7(n2853)*	5.8	0.8	0.13	n.s.	3.8	0.6	0.17	****	9.6	0.9	0.09	18	****
L4 to Adult														
RNAi	**Strain**	mean	sd	cv	p	mean	sd	cv	p	mean	sd	cv	n	p
–	wild type	8.1	0.5	0.06	–	2.2	0.4	0.18	–	10.3	0.4	0.05	16	–
nhr-23	wild type	8.4	0.8	0.09	n.s.	4.6	0.7	0.16	****	13.0	1.1	0.08	17	****
–	*let-7(n2853)*†	6.7	0.6	0.09	****	1.6	0.5	0.30	**	8.4	0.6	0.07	17	****
–	*let-7(n2853)*	6.3	0.4	0.08	****	1.5	0.5	0.33	*	7.9	0.6	0.08	15	****
nhr-23	*let-7(n2853)*	6.7	0.6	0.10	****	3.9	0.6	0.16	****	10.6	0.8	0.07	19	n.s.
–	wild type	7.8	0.5	0.07	–	2.2	0.6	0.18	–	10.0	0.5	0.05	20	–
–	*let-7(mg279)*	7.2	0.6	0.08	**	2.2	0.4	0.17	n.s.	9.3	0.6	0.06	20	**
–	*let-7(mg279) mir-84(tm1304)*	6.1	0.9	0.15	****	2.4	0.6	0.25	n.s.	8.5	0.9	0.15	18	****

†Values for one cohort of animals, which is depicted in Figure 1B′.

Supplemental Table 2 – Relates to Figure 3 and Supplemental Figure 4. LCSs found in nematode and vertebrate homologs of *ROR*

Species	Gene	Identifier	3' UTR length*	LCS 3' nt.	TS (kcal/mol)	Alignment (target 3' UTR versus *let-7*)
C. elegans	*nhr-23*	NM_001025806	868	42	-21.8	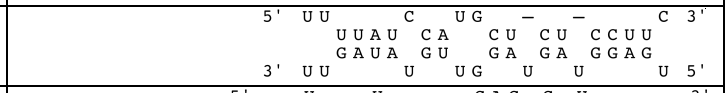
				249	-15.2	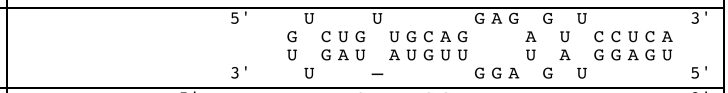
				594	-17.0	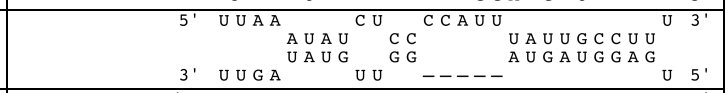
				646	-17.6	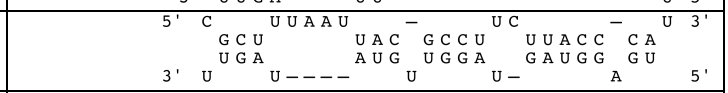
C. briggsae	*nhr-23*	WBGene 00040598	866	629	-20.7	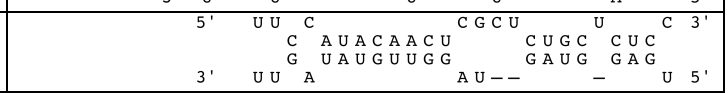
				835	-21.8	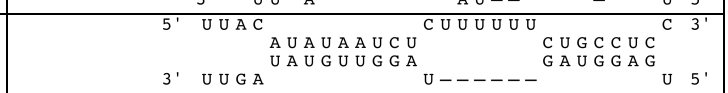
H. sapiens	*RORβ*	NM_006914	7559	3576	-25.9	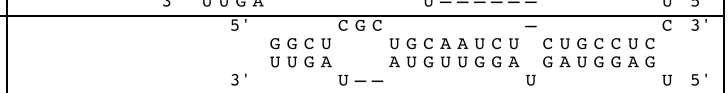
				4055	-23.1	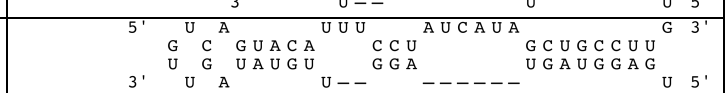
				4961	-23.1	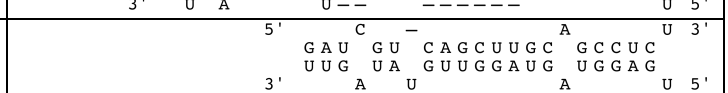
M. musculus	*RORβ*	NM_146095	7271	3817	-23.8	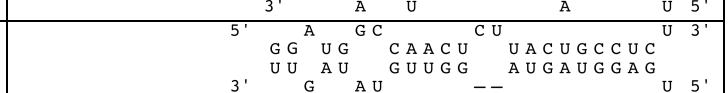
				5242	-22.7	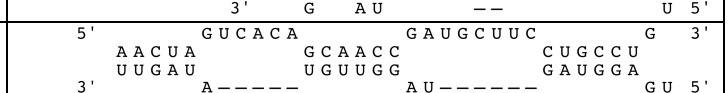
				6675	-26.7	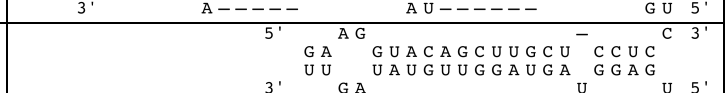
D. rerio	*RORβ*	NM_001082856	5431	949	-21.8	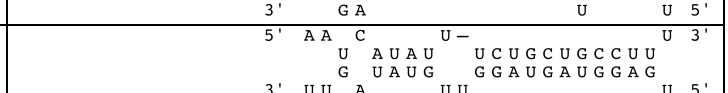
				4318	-23.8	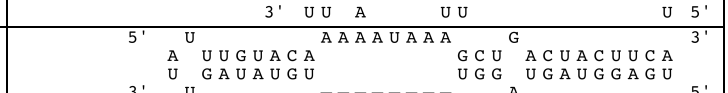
				4421	-23.3	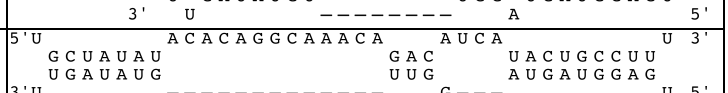
H. sapiens	*RORα*	NM_134261	9171	3079	-23.7	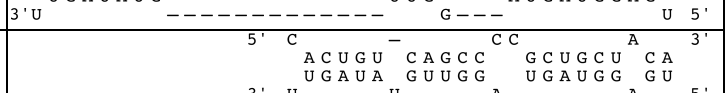
				3142	-22.8	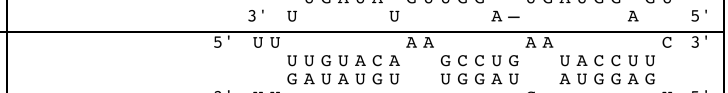
				6480	-24.0	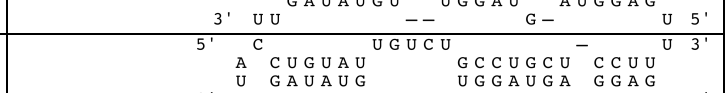
				8321	-22.2	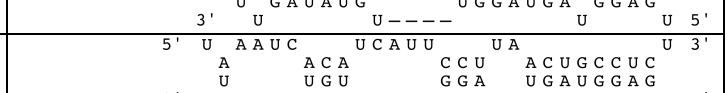
M. musculus	*RORα*	NM_013646	9285	2055	-23.9	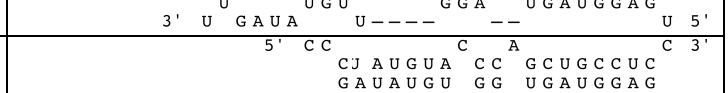
				2184	-23.7	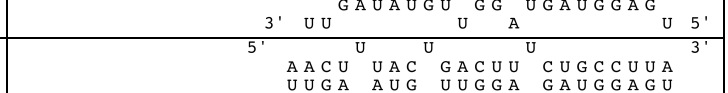
				4913	-22.6	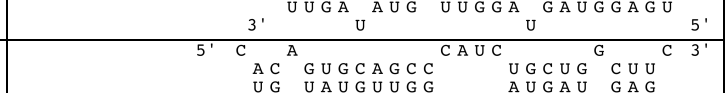

*3' UTRs were supported by ESTs archived in WBcel235/ce11, WBPS9, GRCh38/hg38, GRCm38/mm10, and GRCz10/danRer10.

Supplemental Table 3 – Relates to Figure 4. Classification of genes linked to molting as targets of NHR-23, *let-7s*, neither or both.

Gene Name	Sequence	Criteria for targets of NHR-23:					NHR-23 target (Y/N)	Criteria for targets of *let-7s*:				*let-7s* target (Y/N)	Target class	Cyclic mRNA levels (≈)
		Size of upstream regulatory region & first intron (kb)	RORE #	RORE # Obs. / # Exp.	mRNA levels after *nhr-23* RNAi	NHR-23 ChIP-Seq Peaks (#)		Size of 3' UTR (nt.)	LCS #	LCS # Obs. / # Exp.	ALG-1 iCLIP Peaks (+/-)			
Potential Clock Components														
let-7	C05G5.6	1.5	3	5.8	↓	1	Y	N/A	–	–	–	N/A	NHR-23	≈
lin-42a	F47F6.1	3.7	3	2.3	↓	4	Y	939	4	3.2	+	Y	Shared	≈
lin-42b	F47F6.1	5.5	3	1.6	↓	3	Y	939	4	3.2	+	Y	Shared	≈
lin-42c	F47F6.1	5.5	3	1.6	↓	3	Y	156	0	0	–	N	NHR-23	≈
mir-48	F56A12.3	1.7	2	3.4	–	1	Y	N/A	–	–	–	N/A	NHR-23	≈
mir-241	F56A12.4	2.0	2	2.9	–	2	Y	N/A	–	–	–	N/A	NHR-23	≈
mir-84	B0395.4	2.8	1	1.1	–	2	Y	N/A	–	–	–	N/A	NHR-23	≈
nhr-23	C01H6.5	6.1	8	3.8	↓	3	Y	868	3	2.6	+	Y	Shared	≈
nhr-25	F11C1.6	6.9	3	1.3	–	3	Y	749	1	1.0	+	Y	Shared	≈
Gene Regulatory Factors														
alg-1	F48F7.1	9.9	11	3.2	–	3	Y	400	1	1.9	+	Y	Shared	≈
bed-3	F25H8.6	1.7	2	3.4	–	1	Y	459	1	1.6	+	Y	Shared	≈
blmp-1	F25D7.3	6.7	7	3.0	–	4	Y	861	3	2.6	+	Y	Shared	≈
bro-1	F56A3.5	1.2	0	0.0	–	1	N	379	1	2.0	–	N	–	≈
dre-1	K04A8.6	7.5	8	3.1	–	4	Y	376	2	4.0	+	Y	Shared	≈
mab-10	R166.1	6.0	8	3.9	–	2	Y	374	1	2.0	–	N	NHR-23	≈
nhr-41	Y104H12A.1	11.1	23	6.0	–	2	Y	332	1	2.3	–	N	NHR-23	≈
nhr-67	C08F8.8	5.5	5	2.6	–	0	N	241	3	9.5	–	N	–	–
pqn-47	F59B10.1	5.9	7	3.4	–	5	Y	804	2	1.9	+	Y	Shared	≈
rnt-1	B0414.2	9.2	4	1.3	–	0	N	221	0	0	–	N	–	≈
daf-12	F11A1.3	17.0	12	2.0	–	7	Y	1393	5	2.7	+	Y	Shared	–
gei-8	C14B9.6	1.8	1	1.6	–	3	Y	449	4	6.7	+	Y	Shared	–
skn-1	T19E7.2	5.1	2	1.1	–	2	Y	677	1	1.1	+	Y	Shared	–
Signaling Pathway Components														
acn-1	C42D8.5	4.0	4	2.9	↓	3	Y	384	1	2.0	+	Y	Shared	≈
apl-1	C42D8.8	4.9	4	2.4	–	5	Y	678	1	1.1	+	Y	Shared	≈
calu-1	M03F4.7	1.7	3	5.1	–	3	Y	256	1	3.0	+	Y	Shared	≈
cki-1	T05A6.1	1.9	2	3.1	–	1	Y	235	2	6.5	+	Y	Shared	≈
daf-9	T13C5.1	1.1	0	0.0	↓	1	Y	214	2	7.2	+	Y	Shared	–
glf-1	H04M03.4	2.4	1	1.2	↓	1	Y	247	2	6.2	–	N	NHR-23	≈
lin-3	F36H1.4	5.5	5	1.9	–	0	N	442	5	8.5	+	Y	*let-7s*	–
let-767	C56G2.6	0.6	1	4.8	–	1	Y	87	1	9.2	+	Y	Shared	–
lon-1	F48E8.1	4.8	3	1.8	–	5	Y	185	2	8.3	+	Y	Shared	≈
lrp-1	F29D11.1	7.9	3	1.1	–	6	Y	346	2	4.4	+	Y	Shared	≈
mlt-8	W08F4.6	3.5	2	1.7	↓	1	Y	270	2	5.6	+	Y	Shared	≈
nekl-2	ZC581.1	1.1	1	2.6	–	0	N	73	0	0	–	N	–	≈
nlp-22	T24D8.3	0.8	0	0.0	–	0	N	1000	2	1.5	–	N	–	≈
osm-7	T05D4.4	3.5	1	0.8	–	0	N	121	1	6.5	+	Y	*let-7s*	≈
osm-11	F11C7.5	2.8	1	1.1	–	3	Y	545	4	5.5	+	Y	Shared	≈
phi-59	T19B10.2	1.5	0	0.0	↓	1	Y	121	1	6.5	+	Y	Shared	≈
pod-2a	W09B6.1	3.0	4	3.9	–	2	Y	324	1	2.3	–	N	NHR-23	≈
ptr-4	C45B2.7	4.5	4	2.6	↓	2	Y	221	2	6.9	–	N	NHR-23	≈
ptr-23	ZK270.1	2.0	0	0.0	–	2	N	311	3	7.3	+	Y	*let-7s*	≈
qua-1	T05C12.10	5.7	3	1.5	↓	4	Y	340	1	2.2	+	Y	Shared	≈
	E03H4.8	3.4	1	0.9	–	0	N	307	1	2.5	–	N	–	≈
	T19A5.3	4.9	2	1.2	↓	2	Y	347	1	2.2	+	Y	Shared	≈
	Y47D3B.1	4.9	3	1.8	–	1	Y	98	1	8.1	–	N	NHR-23	≈
Extracellular Matrix Proteins and Receptors														
adt-2	F08C6.1	7.6	7	2.7	–	6	Y	621	1	1.2	+	Y	Shared	≈
bli-5	F45G2.5	1.4	0	0.0	–	0	N	300	1	2.5	+	Y	*let-7s*	≈
bus-8	T23F2.1	3.6	0	0.0	↓	0	N	453	2	3.3	–	N	–	≈
clc-1	C09F12.1	5.4	0	0.0	–	0	N	101	1	7.8	–	N	–	≈

col-12	F15H10.1	0.7	0	0.0	–	0	N	101	1	7.8	+	Y	*let-7s*	≈
dpy-13	F30B5.1	3.8	5	3.8	–	4	Y	63	2	26.1	+	Y	Shared	≈
dpy-17	F54D8.1	0.4	1	7.3	–	0	N	54	1	15.5	–	N	–	≈
dpy-4	Y41E3.2	2.4	0	0.0	–	1	N	102	1	7.8	+	Y	*let-7s*	≈
dpy-5	F27C1.8	0.8	1	3.6	↓	1	Y	39	0	0	–	N	NHR-23	≈
dpy-7	F46C8.6	0.7	2	8.3	↓	1	Y	236	1	3.2	–	N	NHR-23	≈
fbn-1	ZK783.1	8.3	12	4.2	↓	6	Y	457	1	1.7	+	Y	Shared	≈
ina-1	Y116A8A.9	8.0	8	2.9	–	2	Y	261	1	2.9	+	Y	Shared	≈
mam-1	ZC13.3	3.8	3	2.3	–	0	N	243	0	0	–	N	–	≈
mlt-10	C09E8.3	8.6	4	1.3	↓	1	Y	139	2	11.2	+	Y	Shared	≈
mlt-11	W01F3.3	5.2	11	6.1	↓	4	Y	353	1	2.1	+	Y	Shared	≈
mlt-7	ZK430.8	11.5	15	3.8	–	1	Y	317	2	4.8	+	Y	Shared	≈
mlt-9	F09B12.1	3.5	1	0.8	↓	5	Y	313	1	2.4	–	N	NHR-23	≈
mup-4	K07D8.1	5.8	5	2.5	–	2	Y	394	0	0	–	N	NHR-23	≈
nas-36	C26C6.3	1.1	1	2.6	↓	0	Y	327	5	11.6	+	Y	Shared	≈
nas-37	C17G1.6	3.6	7	5.6	↓	2	Y	240	4	12.7	–	N	NHR-23	≈
noah-1	C34G6.6	7.9	9	3.3	↓	5	Y	550	1	1.4	+	Y	Shared	≈
noah-2	F52B11.3	8.9	3	1.0	↓	6	Y	316	2	4.8	+	Y	Shared	≈
pan-1	M88.6	2.5	2	2.3	–	2	Y	393	2	3.8	+	Y	Shared	≈
pat-2	F54F2.1	4.0	4	2.9	–	2	Y	292	2	5.2	+	Y	Shared	≈
rol-6	T01B7.7	3.4	2	1.7	↓	4	Y	117	1	6.7	+	Y	Shared	≈
pat-3	ZK1058.2	5.0	0	0.0	–	2	N	400	1	1.9	+	Y	*let-7s*	≈
Cytoskeletal Components														
ifa-2	W10G6.3	1.7	1	1.7	–	1	Y	186	2	8.3	–	N	Shared	≈
ifc-2	M6.1	3.0	0	0.0	–	0	N	536	2	2.8	+	Y	*let-7s*	≈
nmy-2	F20G4.3	1.8	6	9.7	–	1	Y	448	2	3.4	+	Y	Shared	≈
Randomly Selected Genes with no Known Link to Molting														
acs-13	Y65B4BL.5	4.9	3	1.8	–	2	Y	424	1	1.8	+	Y	Shared	–
ced-8	F08F1.5	0.7	0	0.0	–	0	N	85	0	0	–	N	–	–
cyp-33C12	Y5H2B.6	1.5	0	0.0	–	0	N	148	0	0	–	N	–	–
ech-5	F56B3.5	0.5	0	0.0	–	1	N	602	1	1.2	–	N	–	–
map-2	Y116A8A.9	1.5	1	1.9	–	0	N	274	2	5.6	–	N	–	–
mpst-7	R186.6	1.0	0	0.0	–	1	N	84	0	0	+	N	–	–
nhr-176	F14H3.11	0.2	0	0.0	–	0	N	54	1	15.5	–	N	–	–
nlp-37	F48B9.4	2.9	3	3.0	–	0	N	302	2	5	–	N	–	–
srz-10	ZK1037.11	1.1	1	2.6	–	0	N	16	0	0	–	N	–	–
slc-36.5	C44B7.6	2.4	3	3.6	–	1	Y	74	0	0	–	N	NHR-23	≈
ttll-12	D2013.9	0.1	0	0.0	–	0	N	175	1	4.4	+	Y	*let-7s*	–
unc-112	C47E8.7	2.8	1	1.1	–	1	Y	295	1	2.6	+	Y	Shared	–
	C01G6.9	0.1	0	0.0	–	0	N	76	1	10.6	–	N	–	–
	C06E1.7	2.4	1	1.2	–	1	Y	151	3	15.4	–	N	NHR-23	≈
	F44E5.5	0.4	0	0.0	–	1	N	39	0	0	–	N	–	–
	R10E8.6	1.3	0	0.0	–	0	N	31	0	0	–	N	–	–
	R12B2.2	0.5	0	0.0	–	0	N	115	0	0	–	N	–	–
	T06D4.1	2.3	3	3.8	–	0	N	234	0	0	–	N	–	–
	T19D12.4	2.3	0	0.0	–	0	N	115	0	0	–	N	–	≈
	Y53C10A.6	6.3	0	0.0	–	0	N	201	2	7.6	–	N	–	–